



1 **Drivers of the $\delta^{18}\text{O}$ Changes in Indian Summer Monsoon Precipitation between**
2 **the Last Glacial Maximum and Pre-industrial Period**

3

4 Thejna Tharammal ^{1*}, Govindasamy Bala², Jesse Nusbaumer³

5

6 ¹ Interdisciplinary Centre for Water Research, Indian Institute of Science, Bengaluru
7 560012, India

8 ² Centre for Atmospheric and Oceanic Sciences, Indian Institute of Science,
9 Bengaluru 560012, India

10 ³ National Center for Atmospheric Research, Boulder, USA

11 Corresponding author: thejnat@iisc.ac.in

12

13

14

15

16

17

18

19

20

21

22

23

24

25

26

27

28

29

30

31



32 **Abstract**

33 In this study, we investigate the changes in water isotope ratios in the Indian summer
34 monsoon precipitation ($\delta^{18}\text{O}_{\text{precip}}$) during the Last Glacial Maximum (LGM, ~21 ka
35 Before Present) compared to the pre-industrial (PI) period, and the mechanisms
36 driving these changes, using a general circulation model with water isotope and
37 novel water vapor source-tagging capabilities.

38 During the LGM, the model simulates a substantial reduction (15%) in monsoon
39 precipitation over the Indian subcontinent, consistent with proxy records. This drying
40 in LGM is associated with reduced atmospheric water vapor, a thermodynamic
41 response to cooling, while the westerly circulation, a dynamics response, is
42 strengthened over parts of the subcontinent. Additionally, zonal temperature
43 gradients between a relatively less-cooled tropical Western Pacific Ocean and Indian
44 subcontinent lead to anomalous subsidence over the Indian region, enhancing the
45 drying. Water vapor source tagging shows that while the four dominant moisture
46 sources for the monsoon (South Indian Ocean, Arabian Sea, Indian land recycling,
47 and Central Indian Ocean) remained the same, their contributions were reduced
48 during the LGM. The $\delta^{18}\text{O}_{\text{precip}}$ values over the Indian monsoon region are enriched
49 by approximately 1‰ in the LGM simulation, and we find that this enrichment was
50 not driven by the local amount effect. A decomposition analysis shows that the
51 enrichment was primarily caused by reduced contributions from distant, isotopically
52 depleted water vapor sources and secondarily by reduced rainout during moisture
53 transport from the Indian Ocean.

54 These findings have important implications for paleoclimate reconstructions,
55 suggesting that $\delta^{18}\text{O}$ records from the Indian region could be indicators of broad-
56 scale atmospheric circulation rather than being direct proxies for local precipitation
57 amount.

58
59
60
61



62 **1. Introduction**

63 The Indian summer monsoon (ISM) system, occurring during the months of June-
64 September, is one of the major climate features in the world. It sustains the
65 livelihoods of more than a billion people in the subcontinent by contributing almost
66 80% of the annual precipitation in the region. Monsoons were historically viewed as
67 regional sea breezes driven by differential heating of land and sea. However, they
68 are now understood as interconnected components of a global monsoon system,
69 driven by the migration of Intertropical Convergence Zone (ITCZ), influencing tropical
70 and subtropical precipitation (Gadgil 2003; Geen et al. 2020).

71

72 Recent decades have seen increasing ISM intensification, characterized by more
73 frequent extreme rainfall events and increased variability, likely due to anthropogenic
74 climate change (Krishnan et al. 2016, 2020; Wang et al. 2020; Chen et al. 2020;
75 Katzenberger et al. 2021; Kong et al. 2022; Mukherjee et al. 2024). However, there
76 is considerable uncertainty in these future projections (Krishnan et al. 2020). Even
77 small changes in the monsoon patterns can adversely affect the annual rainfall
78 (~10% reduction in the ISM precipitation from the mean is classified as drought;
79 Shewale and Kumar 2005), hence, it is important to understand the changes and
80 variability in the monsoon rainfall. Paleoclimate studies using climate archives and
81 proxy records provide crucial constraints for reducing uncertainties in future climate
82 projections (Tierney et al. 2020; Lohmann et al. 2020; Rehfeld et al. 2020; Brovkin et
83 al. 2021; Kageyama et al. 2024). They are useful to understand the sensitivity of the
84 monsoon systems to climate factors such as changes in greenhouse gases (GHG),
85 orbital parameters, continental ice sheets, and Sea Surface Temperature (SST).

86

87 The Last Glacial Maximum-LGM, about 23000 to 19000 years before present, is a
88 period of high interest in climate change studies. LGM presents a valuable case
89 study for understanding how the Earth's climate system responded to the influence
90 of reduced CO₂, presence of the Laurentide ice sheets and ice-sheet topography,
91 and orbital forcing. The abundance of proxy-climate records for this period facilitates
92 comparisons between proxy data and models. Climate records from the Indian
93 Summer Monsoon region such as, water isotope records from sedimentary cores
94 and speleothems (Contreras-Rosales et al. 2014; Sinha et al. 2015; Kathayat et al.



2016; Liu et al. 2021) indicate that LGM was characterised by a weaker Indian Summer Monsoon. Climate modeling studies suggest that the general reduction in precipitation over the globe during the LGM is mainly due to the cooling driven by lower greenhouse gas concentrations and the expansion of ice sheets (Broccoli and Manabe 1987, 2008; Yanase and Abe-Ouchi 2007; Tharammal et al. 2013; Kageyama et al. 2020; McGee 2020; Seltzer et al. 2024). Further, the associated cooler sea surface temperatures in the tropics during the LGM (MARGO Project Members 2009; DiNezio et al. 2018; Tierney et al. 2020) likely influenced the strength of the monsoon circulation, weakening the precipitation.

Stable isotopes of water undergo temperature-dependent fractionation during phase changes. The resulting variations in the ratios of heavy to light isotopes (δ -values) serve as powerful tracers of hydrological and atmospheric processes (Galewsky et al. 2016; Dee et al. 2023; Bailey et al. 2024). Records of water isotopes in the climate archives such as speleothems, tree rings, and sediment records are one of the major proxies in reconstructing the Indian monsoon precipitation (Yadava et al. 2004; Maher 2008; Contreras-Rosales et al. 2014; Sinha et al. 2015; Kathayat et al. 2016). To interpret these climate records, *the amount effect* (Dansgaard 1964), which is the observed inverse relationship between the ratio of water isotopes in precipitation ($\delta^{18}\text{O}_{\text{precip}}$) and the amount of precipitation in the tropical regions, is used. The amount effect is related to depletion of water vapor of heavier isotopes during intense precipitation events, especially in convectively active tropical monsoon regions (Risi et al. 2008; Lee et al. 2008; Tharammal et al. 2017). However, the local precipitation amount is not the only factor that determines the isotopic composition of precipitation in the tropics. It is also influenced by other factors such as, relative contributions of moisture from various water vapor sources, atmospheric circulation, and upstream convection (Lewis et al. 2010; Breitenbach et al. 2010; Pausata et al. 2011; Sjolte and Hoffmann 2014; Zhu et al. 2017; Tabor et al. 2018; Konecky et al. 2019; Hu et al. 2019; Tharammal et al. 2023; Chakraborty et al. 2025). This complexity leads to considerable uncertainty in interpreting $\delta^{18}\text{O}$ records from the ISM region. Further, uncertainties remain in inferring the water isotope proxy records due to low data resolution and sparse coverage.

127



128 While proxy records have been used to study past changes in the Indian monsoon
 129 (Yadava et al. 2004; Dutt et al. 2015; Sinha et al. 2015; Kathayat et al. 2016;
 130 Kaushal et al. 2018), climate model studies focussed on the Indian monsoon
 131 precipitation and water isotope ratios during the LGM are largely lacking. Recent
 132 advancements in climate models equipped with water isotope tracers in their
 133 hydrology, along with the capabilities of tracking the evaporative water (Brady et al.
 134 2019) will enable us to find the climatic factors affecting the $\delta^{18}\text{O}_{\text{precip}}$ of monsoon
 135 precipitation, and also differentiate the moisture sources and their effects on the
 136 $\delta^{18}\text{O}_{\text{precip}}$ (Hu et al. 2019; Kathayat et al. 2021; He et al. 2021; Tharammal et al.
 137 2023). Therefore, applying these novel modeling techniques to resolve the drivers of
 138 $\delta^{18}\text{O}_{\text{precip}}$ change in the Indian region during the LGM is a key research gap that this
 139 study aims to fill.

140
 141 In this study, we examine the mechanisms behind the changes in the monsoon
 142 precipitation and water isotope ratios in the ISM region during the LGM using a
 143 climate model with water isotope and novel water vapor source-tagging capabilities.
 144 We will analyse the responses of water isotopes in precipitation, and moisture
 145 sources to the glacial climate, and importantly, identify the major physical processes
 146 influencing the changes in the isotopic ratios of precipitation. We will analyse the
 147 relative importance of the "amount effect" compared to changes in moisture source
 148 and transport in influencing the $\delta^{18}\text{O}_{\text{precip}}$ values during the LGM.

149
 150 The paper is structured as follows: In Section 2, we introduce the model simulations
 151 and methods. Section 3 includes the assessment of model performance under the PI
 152 climate, analysis of changes in the monsoon, water vapor sources, and isotope
 153 ratios of precipitation in the LGM simulation. Section 4 includes a discussion of the
 154 results and main conclusions of the study.

155

156 **2. Methods**

157 **2.1 Climate Model**

158 Our study uses the Community Earth System Model, CESM version 1.2 with water
 159 isotope tracking capabilities (iCESM, Brady et al. 2019) from the National Center for



160 Atmospheric Research (NCAR) for the climate simulations. Atmospheric and land
 161 components of the iCESM are isotopic versions of the Community Atmosphere
 162 Model CAM version 5.3 and Community Land Model CLM version 4, respectively.
 163 The sea-ice model in the iCESM is Los Alamos Sea Ice Model version 4 (CICE4),
 164 which is run in prescribed sea ice mode for the simulations presented here. The
 165 isotope tracking in the model is facilitated with the inclusion of a parallel hydrologic
 166 cycle for the water isotope tracers in the iCESM. It follows the water isotope ratios,
 167 fluxes, and isotopic fractionations on phase changes in the components of the
 168 hydrologic cycle (Brady et al. 2019).
 169 iCESM has proven successful in reproducing the present global distribution of
 170 isotopes in precipitation (Brady et al. 2019). Further, the model includes a tagging
 171 feature for the evaporated water and can be used to track the sources of water vapor
 172 for precipitation in a sink region. The model was successfully used in several studies
 173 to reconstruct the past and present climate and isotope ratios in precipitation, and to
 174 track the sources of water vapor in various tropical regions (Tabor et al. 2018; Hu et
 175 al. 2019; Windler et al. 2020; He et al. 2021; Tharammal et al. 2023).

176

177 **2.2 Experiments**

178 We conducted two time-slice simulations for the current study, a) the pre-industrial
 179 (PI) control experiment and b) the LGM simulation, with prescribed SSTs, sea ice
 180 extent, and prescribed ocean surface isotopic ratios.

181 The isotopic composition of meteoric water is represented by the delta (δ) value in
 182 permil (‰) units in the paper, denoting the relative abundance of the ratio of heavy
 183 isotope to the light isotope in a sample with respect to a geochemical standard
 184 (VSMOW-Vienna Standard Mean Ocean Water).

185 Accordingly, $\delta^{18}\text{O}$ is $(R_{\text{sample}}/R_{\text{VSMOW}} - 1) \times 1000$. R is the ratio of heavy to the light
 186 isotope, $^{18}\text{O}/^{16}\text{O}$. R_{VSMOW} is the standard isotope ratio.

187

188 For the PI simulation, the orbital conditions, GHG, SST, sea ice extent, and aerosol
 189 boundary conditions are set at the year 1850. The GHG and orbital boundary
 190 conditions of the experiments are given in Table S1. The SST and sea ice fraction
 191 data for the PI experiment are derived from the corresponding coupled CESM



192 simulation (Zhu and Poulsen 2021). A uniform sea-surface $\delta^{18}\text{O}$ of 0.5‰ is
 193 prescribed for the control simulation. This is an approximate value based on present-
 194 day observations and is close to the observed surface values of the tropical and
 195 subtropical oceans (Hoffmann and Heimann 1997; LeGrande and Schmidt 2006; Lee
 196 and Fung 2008).
 197 For the LGM simulation, we follow the Paleoclimate Modelling Intercomparison
 198 Protocol version 4 (PMIP4; Kageyama et al. 2020), and the GHG, orbital parameters,
 199 land-sea mask, and surface topography are set to 21 ka BP conditions. The ice
 200 sheet extent and topography for the LGM experiment (Fig. S1a) are derived from the
 201 ICE-6G ice sheet reconstructions by Peltier et al. (2015). The coastlines for the LGM
 202 experiment are adapted from the ICE-6G reconstruction and represent a lowering of
 203 sea level by 120m during the LGM (Lambeck et al. 2014). The SST and sea ice
 204 fraction for the LGM simulation (Fig. S1b, c) are obtained from the CESM coupled
 205 LGM simulation (Zhu and Poulsen 2021). The formation of large continental ice
 206 sheets during the LGM led to enrichment of heavier isotopes in the seawater oxygen
 207 isotope ratios (ice-volume effect, Lambeck 2000). It is widely accepted that the sea
 208 surface water isotope ratios during the LGM were approximately 1‰ enriched
 209 compared to the pre-industrial values (Sima et al. 2006; Duplessy et al. 2002). We
 210 represent this in the LGM simulation by prescribing a uniform sea surface
 211 enrichment of water isotopes by 1‰ for $\delta^{18}\text{O}$, compared to the PI value.
 212 Further, to identify the effects of water vapor sources on the monsoon precipitation
 213 and water isotopes during the LGM, we tag the evaporated vapor from 17 ocean and
 214 land regions in and around the ISM region in both the PI and the LGM experiments
 215 (tagged regions are shown in Fig. S2a). The simulations are run for 30 years, and
 216 the last 20 years are used for the analysis.

217

218 **2.3 Monsoon circulation indices and moisture budget analysis**

219 **2.3.1 Monsoon circulation indices**

220 Strength of the monsoon circulation can be estimated using various indices (Li et al.
 221 2024). We calculate the monsoon circulation strength in PI and LGM simulations
 222 using the following six indices selected to capture both circulation changes and water
 223 vapor transport related to the monsoon precipitation. The geographical domains
 224 used for the estimation of these indices are shown in Figure S2b.



225 1) The Somali jet index (Boos and Emanuel 2009), which is calculated as the square
 226 root of twice the domain mean kinetic energy ($\sqrt{2\overline{KE}}$) of the 850 hPa horizontal
 227 wind over the region, [5°S - 20°N, 50°E - 70°E].

228

229 2) The hydrological index, following (Fasullo and Webster 2003), calculated by
 230 averaging the Vertically Integrated Moisture Transport (VIMT) in the Indian Ocean-
 231 Arabian Sea region, [20°S-30°N, 40°E-100°E]. VIMT is the total horizontal movement
 232 of water vapor in a vertical column of the atmosphere, and we calculate the term
 233 from the surface up to 300 hPa.

$$234 \quad VIMT = \frac{1}{g} \int_{P_{surface}}^{P_{top}} qV dp \quad \text{----- (1)}$$

235

236 Magnitude of VIMT is,

$$237 \quad |VIMT| = \sqrt{VIMT_u^2 + VIMT_v^2} \quad \text{----- (2)}$$

238 Where P is atmospheric pressure, g is gravity, q is the specific humidity, and V is the
 239 wind vector with zonal and meridional components u and v.

240 3) Mid-tropospheric temperature gradient (ΔTT), defined as the tropospheric
 241 temperature difference between a northern region and a southern region in the larger
 242 monsoon domain (Xavier et al. 2007). ΔTT signifies the cross-equatorial temperature
 243 gradient, and the onset of the ISM is defined as the time when ΔTT changes from
 244 negative to positive.

245 4) The vertical shear of zonal winds, following (Webster and Yang 1992), calculated
 246 as the difference between 200 hPa and 850 hPa zonal winds (U200-U850),
 247 averaged over the region 10°N-30°N, 50°E-95°E.

248 5) The meridional shear of the 850 hPa zonal wind (barotropic shear, $-\partial u/\partial y$) over the
 249 region 10°N-26°N, 70°E-90°E that indicates magnitude of the cyclonic shear of the
 250 low-level monsoon circulation.

251 6) Various studies (Xue et al. 2003; Kripalani et al. 2007; P J et al. 2020; Azhar et al.
 252 2023) highlight a strong dependence of ISM circulation strength on the sea level
 253 pressure difference between the Mascarene High in the Southern Indian Ocean (MH;
 254 20°S-40°S, 45°E-100°E) and the wider ISM region (10°N-35°N, 45°E-100°E).
 255 Therefore, this sea level pressure difference is also treated as an ISM index for this
 256 study.



2.3.2 Moisture budget calculations

To understand the mechanisms driving the changes in monsoon precipitation, we conducted a moisture budget analysis based on the framework of Chou and Lan (2012). In this analysis, the net precipitation over a region (Precipitation-Evaporation, P-E) is balanced by the vertically integrated moisture flux convergence in steady state conditions.

This convergence term is then decomposed into contributions from vertically integrated horizontal advection (the transport of water vapor, q , by horizontal winds, $-[u(\partial q/\partial x) + v(\partial q/\partial y)]$) and the transport of moisture by vertical atmospheric motion, vertical advection $(-\omega(\partial q/\partial p))$.

$$P-E = -\langle u(\partial q/\partial x) + v(\partial q/\partial y) \rangle - \langle \omega(\partial q/\partial p) \rangle, \quad (3)$$

The brackets $\langle \rangle$ denote pressure, mass-weighted vertical integration. u , v , and ω are the zonal, meridional, and vertical wind components.

A further decomposition of the advection terms into thermodynamic and dynamic components to differentiate the contributions from the changes in water vapor and circulation (e.g., Chou et al. 2009; Chou and Lan 2012) was not performed, as it is beyond the scope of this study.

2.4 Decomposition of $\delta^{18}\text{O}_{\text{precip}}$ changes

To diagnose the mechanisms driving the changes in precipitation-weighted $\delta^{18}\text{O}_{\text{precip}}$ in the ISM region between the LGM and PI simulations, we perform a decomposition analysis following the framework of Tabor et al. (2018). Using our water vapor tagging results, this method expresses the total change in precipitation-weighted $\delta^{18}\text{O}_{\text{precip}}$ ($\delta^{18}\text{O}_p$ in the equations below) in the ISM domain as the sum of contributions from each of the 17 tagged source regions.

$$\Delta \delta^{18}\text{O}_p = \sum_{i=1}^{i=17} \left[\left(\delta^{18}\text{O}_{p_i} \times \frac{p_i}{p_{\text{total}}} \right)_{LGM} - \left(\delta^{18}\text{O}_{p_i} \times \frac{p_i}{p_{\text{total}}} \right)_{PI} \right] \quad (4)$$



286 where $\delta^{18}\text{O}_{\text{pi}}$ is the isotopic ratio of precipitation at the ISM domain of water vapor
 287 source i , and (p_i/p_{total}) is the relative contribution of precipitation from source i to the
 288 total precipitation at the ISM domain.

289 Further, the decomposition method isolates two primary effects on the change in
 290 each $\delta^{18}\text{O}_{\text{pi}}$ between LGM and PI: 1) contributions from changes in the isotopic
 291 composition of each source tag between LGM and PI (First term on the right in Eqn.
 292 5), and 2) the effect of changes in the relative precipitation contribution from the
 293 water vapor sources (Second term on the right in Eqn. 5).

$$\Delta(\delta^{18}\text{O}_p)_i = \underbrace{(\delta^{18}\text{O}_{p_i, \text{LGM}} - \delta^{18}\text{O}_{p_i, \text{PI}})}_{\text{Change in Isotopic Value}} \times \left(\frac{p_i}{p_{\text{total}}}\right)_{\text{PI}} + \delta^{18}\text{O}_{p_i, \text{PI}} \times \underbrace{\left(\left(\frac{p_i}{p_{\text{total}}}\right)_{\text{LGM}} - \left(\frac{p_i}{p_{\text{total}}}\right)_{\text{PI}}\right)}_{\text{Change in Relative Precipitation Contribution}}$$

294
 295 --(5)

296 For each tag, the first term on the right can further be decomposed to three isotopic
 297 effects: (i) the source effect, due to changes in $\delta^{18}\text{O}$ of water vapor at the source
 298 region, (ii) rainout effect, the changes in $\delta^{18}\text{O}_{\text{pi}}$ of source tags due to changes in
 299 rainouts on the path, and (iii) condensation effect, the enrichment of $\delta^{18}\text{O}_{\text{pi}}$ at the sink
 300 during condensation from the ambient vapor. The three terms are calculated as:

$$\Delta\delta^{18}\text{O}_{\text{source}, i} = (\delta^{18}\text{O}_{wv_{\text{source}}, \text{LGM}} - \delta^{18}\text{O}_{wv_{\text{source}}, \text{PI}}) \times \left(\frac{p_i}{p_{\text{total}}}\right)_{\text{PI}} \quad \text{--- (6)}$$

301
 302

$$\Delta\delta^{18}\text{O}_{\text{rainout}, i} = [(\delta^{18}\text{O}_{wv_{\text{sink}}} - \delta^{18}\text{O}_{wv_{\text{source}}})_{\text{LGM}} - (\delta^{18}\text{O}_{wv_{\text{sink}}} - \delta^{18}\text{O}_{wv_{\text{source}}})_{\text{PI}}] \times \left(\frac{p_i}{p_{\text{total}}}\right)_{\text{PI}}$$

303
 304 - (7)

$$\Delta\delta^{18}\text{O}_{\text{condensation}, i} = [(\delta^{18}\text{O}_{p_{\text{sink}}} - \delta^{18}\text{O}_{wv_{\text{sink}}})_{\text{LGM}} - (\delta^{18}\text{O}_{p_{\text{sink}}} - \delta^{18}\text{O}_{wv_{\text{sink}}})_{\text{PI}}] \times \left(\frac{p_i}{p_{\text{total}}}\right)_{\text{PI}}$$

305
 306 -- (8)

307 $\delta^{18}\text{O}_{wv_{\text{source}}}$ and $\delta^{18}\text{O}_{wv_{\text{sink}}}$ are the isotope ratios of water vapor at 850 hPa
 308 (representing low level vapor, also level of monsoon low-level jet) of each tag at their
 309 source and at the Indian sink, respectively.

310 Hence, we can quantitatively assess the driving mechanisms responsible for the
 311 difference in total precipitation $\delta^{18}\text{O}_{\text{precip}}$ between the LGM and PI climates.



312 **3. Results**

313 **3.1 PI control simulation**

314 **3.1.1 Monsoon in the PI control climate**

315 The model successfully simulates both the annual cycle and the summer monsoon
 316 (mean of June-July-August-September, JJAS) precipitation, also the south westerly
 317 winds over the ISM domain (8°N-30°N and 65°E-88°E; Fig. 1). The summer
 318 monsoon precipitation accounts for approximately 80% of the total annual
 319 precipitation, in agreement with the GPCP observational data (Adler et al. 2018).
 320 However, the iCESM overestimates the summer monsoon precipitation by ~20%
 321 (Fig. 1c). This wet bias has been reported in previous studies that used the CESM
 322 model (e.g. Pathak et al. 2019; Hanf and Annamalai 2020) and they attribute this
 323 bias to factors such as, model resolution, biases in simulated circulation, and
 324 convective parameterizations.

326 **3.1.2 Water isotopes in the PI monsoon precipitation**

327 The domain mean water isotope ratio of precipitation (precipitation weighted,
 328 $\delta^{18}\text{O}_{\text{precip}}$, Fig. 2a) over the ISM region during the JJAS season in the PI simulation is
 329 -7‰. This is considerably more negative than the mean of -3.7‰ calculated from the
 330 available GNIP observational data over the domain (Fig. 2a). A likely reason for the
 331 more negative $\delta^{18}\text{O}_{\text{precip}}$ values simulated in the ISM region is the wet bias in the
 332 model (Fig. 1c) and consequent depletion of the heavier isotopes, as also suggested
 333 by previous studies using isotope-enabled CAM and iCESM models (Nusbaumer et
 334 al. 2017; Tharammal et al. 2017; Tharammal et al. 2023). It should be noted,
 335 however, that a lack of wider observational networks and continuous monitoring of
 336 seasonal $\delta^{18}\text{O}_{\text{precip}}$ values hinder a comprehensive comparison of the observations
 337 and our simulation.

338
 339 In the PI simulation, the linear regression analysis between the JJAS mean $\delta^{18}\text{O}_{\text{precip}}$
 340 values and the precipitation amount show a moderate amount effect in the ISM
 341 region (-0.22‰/mm day⁻¹ slope of the spatial amount effect, the square of the
 342 Pearson correlation coefficient r^2 0.37, Fig. S3). The moderate strength of this



relationship, which is physically related to rainout during heavy rainfall and convective events (Risi et al. 2008; Tharammal et al. 2017; Lee and Fung 2008), suggests that factors other than local precipitation amount also strongly influence the simulated $\delta^{18}\text{O}_{\text{precip}}$ values. These may include large-scale circulation, upstream convection, or the effects of water vapor sources with differing isotope signatures (Pausata et al., 2011; Risi et al., 2008; Tharammal et al., 2023), as discussed in the following section.

3.1.3 Water vapor sources and their effect on $\delta^{18}\text{O}_{\text{precip}}$ in the PI climate

We used source water tagging to identify the primary water vapor sources for ISM precipitation in the PI simulation. Our simulation shows that the 17 tagged source regions (Fig. S2) contribute approximately 96% of the total JJAS precipitation (Fig. 2b). Four major sources- the South Indian Ocean (SIO) and Central Indian Ocean- CIO (22% and 10% respectively), Arabian Sea (19%), and Indian land recycling (17%), together account for ~68% of the total precipitation. The Bay of Bengal (BOB) contributes only ~3% to the ISM precipitation. These results are consistent with previous water vapor tracking studies in the ISM domain using Lagrangian models (e.g. Gimeno et al. 2010, 2012; Ordóñez et al. 2012; Pathak et al. 2014; Dey and Döös 2021) and present-day results using the iCESM model (Tharammal et al. 2023).

The precipitation contribution-weighted sum of $\delta^{18}\text{O}_{\text{pi}}$ of all the 17 tags at the sink (-6.7‰, based on Eqn. 4) explains ~95% of the domain mean $\delta^{18}\text{O}_{\text{precip}}$ in the ISM region (-7‰, cf. 3.1.2), which validates our source-tagging framework (Eqn. 4, Fig. 2c). The results show substantial differences in the isotope signatures between the major sources, mainly influenced by transport distance. For instance, while the Arabian Sea and SIO contribute comparably to JJAS precipitation (19% and 22%, respectively), their water isotopic signatures in precipitation ($\delta^{18}\text{O}_{\text{pi}}$) greatly differ. The Arabian Sea source is relatively enriched (-0.1‰ mean over the ISM region), whereas the SIO has much depleted $\delta^{18}\text{O}_{\text{pi}}$ values of -2.5‰ (Fig. 2c). This is likely due to the larger distance of the SIO source from the ISM sink region and consequent depletion of the vapor during condensation and rainouts in the path. Similarly, the evapotranspiration from the ISM land domain, recycling source,



376 contributes 17% to the total precipitation, and the $\delta^{18}\text{O}_{\text{pi}}$ values of recycling are
 377 comparatively enriched (-0.6‰), likely due to being the local source of vapor. Hence,
 378 we suggest that the isotopic composition of ISM precipitation is sensitive to the
 379 relative contributions of these dominant water vapor sources and their isotopic
 380 signatures.

381

382 **3.2 Global climate response in the LGM simulation**

383 In the LGM simulation, the annual global mean surface temperature cooled by
 384 6.75°C compared to the PI (Fig. S4a). While this cooling is consistent with coupled
 385 CESM simulations (-6.8°C ; Zhu et al. 2017; Tierney et al. 2020), it is greater in
 386 magnitude than the PMIP4 multi-model mean (Kageyama et al. 2020). The cooling is
 387 more pronounced over the Laurentide ice sheets and in the polar regions, due to ice
 388 sheet albedo feedback and polar amplification. This leads to an asymmetry in the
 389 annual cooling between the two hemispheres, with Northern Hemisphere (NH)
 390 cooling (-7.5°C) exceeding that of the Southern Hemisphere (SH; -6.0°C)
 391 ($\Delta\text{TS}=1.4^{\circ}\text{C}$). This interhemispheric asymmetry in cooling is smaller than previous
 392 modeling studies that found values more than 3°C (Broccoli, 2000). The simulated
 393 cooling in the high latitude ocean regions (~ 5 to 6°C , Fig. S1a) agrees well with the
 394 proxy-reconstructions (MARGO Project Members 2009). However, the model
 395 simulates colder SSTs in the tropics compared to the MARGO and GLOMAP
 396 reconstructions as noted by previous studies ($\sim 3^{\circ}\text{C}$ in CESM simulations versus
 397 $\sim 1.5^{\circ}\text{C}$; (Tierney et al. 2020).

398

399 Globally, the annual mean precipitation reduces by $\sim 12\%$ (Fig. S4b) in the LGM,
 400 consistent with proxy records and modeling studies including the PMIP4 LGM
 401 simulations (Bartlein et al. 2011; Yan et al. 2016; DiNezio et al. 2018; Kageyama et
 402 al. 2020). This reduction corresponds to a global hydrological sensitivity of $\sim 1.8\%$ per
 403 $^{\circ}\text{C}$ of cooling, and is close to the estimated thermodynamic increase in global
 404 precipitation of 2% per unit increase in temperature (Trenberth 2011). Despite the
 405 reduction in global mean precipitation, an increase in precipitation is simulated in
 406 some regions such as, tropical Pacific, parts of N. America, and South Africa, and
 407 these patterns are also found in the PMIP4 simulations (Kageyama et al. 2020).



408

409 Furthermore, we find that the position of the annual mean Intertropical Convergence
 410 Zone (ITCZ), defined as the median of zonal precipitation (20°S-20°N; McGee et al.
 411 2014; Devaraju et al. 2015), shifts northward by 1.2° in the LGM simulation. This
 412 finding contrasts with the southward shift of ITCZ reported in many of the PMIP4
 413 models (Wang et al. 2023), but is consistent with results from CESM2 (Zhu et al.
 414 2022; Lofverstrom and Zhu 2023) as also reported in Wang et al. (2023).
 415 Lofverstrom and Zhu (2023) attribute this possible bias in the LGM ITCZ shift to
 416 biases in the model's cloud microphysics. It is likely that the simulated northward
 417 displacement of the ITCZ in the LGM in our simulation is due to a robust increase in
 418 precipitation over the northern tropical Pacific, coupled with widespread drying in the
 419 Southern Hemisphere tropical regions (Fig. S4b).

420 **3.3 Indian summer monsoon precipitation during the LGM**

421 The LGM simulation shows a substantial reduction in the Indian summer monsoon
 422 precipitation (Fig. 3), characterized by widespread drying over India, SE Asia, and
 423 Arabian Peninsula region. The precipitation amount is reduced by ~15% over the
 424 ISM domain, which is notable since a precipitation deficit exceeding 10% from the
 425 long-term mean is considered drought conditions in India (Shewale and Kumar
 426 2005). The ISM precipitation responses in the LGM simulation are broadly consistent
 427 with both monsoon proxy-records and previous climate model simulations (Jiang et
 428 al. 2015; Dutt et al., 2015; Yan et al. 2016; Kageyama et al. 2020). The large-scale
 429 drying is primarily due to regional and global cooling in both annual and summer
 430 means (Fig. S4a, S5a) and generally reduced evaporation from the tropical oceans
 431 (Fig. S5b). These patterns are linked to decreased atmospheric humidity and
 432 reduced column-integrated precipitable water (reduction of 25.2% over the ISM
 433 domain, Fig. S6). However, the drying during the summer monsoon season is not
 434 uniform across the region. Increased precipitation is simulated in the east part of
 435 India and the Bay of Bengal (Fig. 3). As this increase cannot be explained by the
 436 precipitable water anomalies in the LGM (Fig. S6), it is likely driven by changes in
 437 atmospheric circulation.



3.3.1 Monsoon circulation changes in the LGM and moisture budget

The LGM simulation shows a weakening of the low-level (850 hPa) westerly circulation and wind speeds towards land over the Northern Arabian Sea (Fig. 3, Fig. S7b), driven by substantially weakened land-ocean thermal (Fig. S5a, larger cooling over the land) and pressure gradients (S8b; Roxy et al. 2015; Weldeab et al. 2022). Surface cooling over the Indian subcontinent (domain mean -4.5°C ; Table S2) in the LGM is approximately 1°C greater than the sea surface temperature cooling in the neighbouring Arabian Sea, which is consistent with the lower heat capacity of land, leading to more pronounced cooling and enhanced surface pressure over land.

The circulation response is not uniform across the region, as a regional intensification of the low-level westerly winds is simulated across the central and southern parts of India and the Bay of Bengal (Fig. 3, Fig. S7b). This regional intensification of the monsoon circulation is captured by several monsoon circulation indices used in this study- an increased vertical shear of zonal winds, strengthening of the Somali Jet, and enhanced barotropic shear (Fig. S9b, d, f, respectively). We suggest the enhanced westerly circulation in parts of the monsoon region, especially the Somali jet, is influenced by a stronger Mascarene high in the Southern Indian Ocean (Fig. S9e, S8b) that enhances the pressure gradient between the Indian land and the Southern Indian Ocean by ~ 2 mb (Fig. S8b, S9e). The strengthened Mascarene high is a result of the sea ice extension and cooling in the Southern Indian Ocean during the LGM (Fig. S1b, c). This is in agreement with the positive relationship between the ISM circulation and pressure gradient between the Indian monsoon region and the Mascarene high, suggested by several previous studies (Kripalani et al. 2007; P J et al. 2020; Azhar et al. 2023). However, the tropospheric temperature gradient (ΔT), shows a weakening by 2.5% in the LGM. This indicates a weaker thermal forcing of the monsoon, likely due to enhanced cooling in the northern box used for the estimation of ΔT (Fig. S2b, S5a), in the LGM simulation.

We note that the indices related to monsoon circulation (vertical shear of zonal winds, Somali jet speed index, pressure gradient between MH and ISM regions that characterize dynamical responses (Fig. S9) show a general strengthening of the monsoon circulation by $\sim 12\text{-}15\%$ in the LGM simulation, compared to the PI. The



471 barotropic index shows an even larger percentage change between LGM and PI of
 472 >100%. However, the index related to water vapor content and its transport (the
 473 monsoon hydrological index and Vertically Integrated Moisture Transport VIMT that
 474 characterize thermodynamical responses, (Fig. S9c, S10, Fasullo et al. 2003) shows
 475 a reduction by 7.5%, along with a reduction of column-integrated precipitable water
 476 over the ISM region by ~25% (Fig. S6). This shows that the reduction in the ISM
 477 precipitation in the LGM simulation is mainly due to the thermodynamic response to
 478 the cooling (reduced water vapor in the atmosphere), despite an enhanced
 479 dynamical response (circulation changes).

480

481 To understand the drivers of the regional precipitation changes, we analysed the
 482 surface moisture budget (net precipitation, P-E), decomposing it into contributions
 483 from horizontal and vertical advection of moisture (Section 2.3, Chou and Lan,
 484 2012). The analysis (Fig. 4) shows that the major term related to the drying (Fig. 4a)
 485 in the ISM region is the decrease in the horizontal moisture advection (Fig. 4b). This
 486 is due to both the reduction in the moisture availability, and reduced transport as
 487 discussed before. In contrast, the increased precipitation in eastern part of India and
 488 BOB in the LGM is caused by enhanced moisture convergence and vertical
 489 advection (Fig. 4c) linked to the intensified monsoon westerlies in that region. We
 490 note that these results for the advection terms include both dynamic and
 491 thermodynamic responses (Chou and Lan 2012) and delineating them is out of the
 492 scope of this paper.

493

494 The ISM precipitation reductions are also associated with large-scale zonal
 495 temperature gradients between a cold tropical western Pacific Ocean and a relatively
 496 colder Indian subcontinent (Fig. S5a). This leads to anomalous updrafts over the
 497 western Pacific, and increased subsidence over the Indian region (Fig. 5b, Fig.
 498 S11b, d). The relationship between a warmer W. Pacific and drying over the Indian
 499 region is discussed in previous studies (Annamalai et al. 2013). Furthermore, the
 500 Western tropical Pacific is ~1.5°C warmer compared to the Central and Eastern
 501 tropical Pacific in the LGM simulation (Fig. S5a). This intensifies the Pacific Walker
 502 circulation further, and enhances the subsidence and drying over the Eastern Pacific
 503 and the Indian subcontinent in the LGM. We suggest this large-scale circulation
 504 response enhanced the drying over India in the LGM simulation.



505 **3.4 Monsoon water vapor sources under glacial conditions**

506 In the LGM simulation, the major four sources - SIO, Arabian Sea, recycling, and
 507 CIO- remain unchanged (23%, 21%, 19%, and 10% contributions to total
 508 precipitation, respectively) and their relative contributions change by less than 4%
 509 compared to the PI (Fig. 6b). However, the absolute amount of moisture from each
 510 source decreases by 10-14% (Fig. 6a). This reduction is primarily driven by reduced
 511 evaporative fluxes over the source regions (up to ~50% from the PI values; Fig. S5b,
 512 Table S2) and a general weakening of the moisture transport (Fig. S8b). The
 513 reduction in horizontal advection term over the ISM region in the moisture budget
 514 (Fig. 4b) corroborates with these results. This suggests that changes in atmospheric
 515 circulation and cooling of sea surface temperatures during the LGM significantly
 516 impacted the availability and transport of moisture to the Indian monsoon region.

517 **3.5 $\delta^{18}\text{O}_{\text{precip}}$ in the LGM**

518 Globally, the LGM simulation shows a strong depletion in annual mean $\delta^{18}\text{O}_{\text{precip}}$
 519 values (by 5 to >10‰) over the high latitudes and continental ice sheets (Fig. S4c).
 520 This is mainly due to the “temperature effect”, as the cooling in the LGM leads to a
 521 stronger Rayleigh distillation process (Galewsky et al. 2016). Previous studies
 522 (Broccoli and Manabe 2008; Tharammal et al. 2013; Zhu and Poulsen 2021;
 523 Kageyama et al. 2020) have shown that reduced GHG and consequent cooling,
 524 changes in circulation, and both topography and albedo of the ice sheets contribute
 525 to this depletion in the high latitudes. In the following text, we discuss the changes in
 526 $\delta^{18}\text{O}_{\text{precip}}$ over the ISM region during the JJAS season.

527
 528 In contrast to the high latitudes, considerable enrichment of $\delta^{18}\text{O}_{\text{precip}}$ (1‰–4‰) over
 529 tropical regions including the Indian Ocean, Southeast Asia, and ISM regions (mean
 530 enrichment of 0.9‰ over the ISM domain) is simulated in the JJAS season (Fig. 7).
 531 This simulated enrichment is in agreement with the proxy data records from the
 532 South Asian summer monsoon region and climate model simulations (Hoffmann and
 533 Heimann 1997; Tiwari et al. 2011; Liu et al. 2014; Jiang et al. 2015; Kathayat et al.
 534 2016; Kaushal et al. 2018).

535



536 The JJAS mean amount effect in the LGM (spatial slope -0.24 ‰/mmd^{-1} , $r^2=0.30$,
 537 Fig. S3) is moderate and similar to that in the PI simulation. Importantly, the linear
 538 regression analysis (Fig. S3) shows that there is no significant correlation between
 539 the changes in precipitation (ΔP) and the changes in $\delta^{18}\text{O}_{\text{precip}}$ between the LGM and
 540 PI simulations (temporal slope of amount effect, $\Delta\delta^{18}\text{O}_{\text{precip}}/\Delta P$, slope -0.09
 541 ‰/mmd^{-1} , $r^2=0.07$). Hence, the LGM enrichment in the ISM region cannot be
 542 explained by the amount effect, and the results indicate the influence of other factors
 543 such as changes in water vapor sources and atmospheric circulation.

544

545 **3.6 Drivers of monsoon $\delta^{18}\text{O}_{\text{precip}}$ changes: Perspectives from source tagging**

546 To diagnose the physical processes responsible for the changes in the monsoon
 547 $\delta^{18}\text{O}_{\text{precip}}$ during the LGM, we conducted a decomposition analysis of the JJAS mean
 548 LGM-PI $\delta^{18}\text{O}_{\text{precip}}$ anomalies, following (Tabor et al. 2018). Details of the calculations
 549 are given in Section 2.4. Using the results from water tagging experiments, we
 550 separated the anomalies (LGM-PI) in the $\delta^{18}\text{O}_{\text{precip}}$ of each source tag ($\Delta\delta^{18}\text{O}_{\text{pi}}$) into
 551 4 components: 1) effects of changes in source vapor $\delta^{18}\text{O}$ ($\Delta\delta^{18}\text{O}_{\text{source}}$), 2) effects of
 552 changes in rainout during transport ($\Delta\delta^{18}\text{O}_{\text{rainout}}$), 3) effects of changes in
 553 condensation over the Indian monsoon domain ($\Delta\delta^{18}\text{O}_{\text{condensation}}$), and, 4) effects of
 554 changes in the relative contributions of each source to total precipitation over India
 555 (Shown in Fig. 8a-d).

556

557

558 The analysis shows that the dominant contributor to the positive anomalies in the
 559 $\delta^{18}\text{O}_{\text{precip}}$ values over the ISM domain is the change in the relative contribution of the
 560 water vapor sources, which accounts for an enrichment of $+0.6\text{‰}$ (Fig. 8d). This is
 561 caused by a reduction in the relative contribution from remote and depleted water
 562 vapor sources- North and South Pacific, Atlantic, and South China Sea (Fig. 8d).
 563 The second largest positive contribution is from the Rainout Effect ($+0.4\text{‰}$ in total,
 564 Fig. 8b). This is driven by a weaker rainout along transport pathways from major
 565 water vapor sources -Southern and Central Indian Ocean, due to a weaker
 566 circulation in many parts of the Indian Ocean, and overall reduced rainfall in the
 567 LGM. In contrast, the Source Effect (effects of changes in source vapor $\delta^{18}\text{O}$, Fig.
 568 8a) provides a small net negative contribution, as a positive contribution from the



569 Arabian Sea is offset by negative effects from other source regions (Fig. 8a). The
570 positive effect from the Arabian Sea source is likely due to a localized increase in
571 evaporation (Fig. S5b) in contrast to other sources where evaporation was generally
572 reduced, and also the prescribed 1‰ global ocean surface enrichment in the LGM
573 simulation.

574

575 The condensation term, which represents the local enrichment of the precipitation at
576 the sink during the phase transition of vapor to precipitation, produces only a minor
577 and slightly negative contribution (Fig. 8c). This suggests that the isotopic
578 enrichment of precipitation on condensation was weaker in the LGM compared to the
579 PI. This finding also confirms that the amount effect is not a primary driver of the
580 LGM enrichment. If a strong amount effect existed, the reduced LGM precipitation
581 should have produced a positive condensation term. The negative contribution from
582 the condensation term, therefore, agrees with our previous analysis showing no
583 significant temporal correlation between changes in ISM precipitation and isotopes
584 (Section 3.5; Figure S3) in the LGM.

585 **4. Discussion and Conclusions**

586 The present study used a water isotope, water tagging-enabled general circulation
587 model to investigate the Indian summer monsoon precipitation and isotope
588 responses under glacial conditions. Our simulations show a 15% reduction of
589 monsoon precipitation over the Indian domain. Our study shows that the reduction in
590 Indian monsoon precipitation is due to the effects of global cooling and reduced
591 humidity (due to reduced CO₂ and the presence of continental ice-sheets;
592 (Kageyama et al. 2020), and a weakened land-ocean temperature gradient which
593 reduced the strength of the monsoonal circulation in many parts of the ISM region.
594 The LGM drying over the Indian subcontinent was enhanced by a Walker-like
595 circulation response, driven by zonal temperature gradients between the less-cooled
596 Western Pacific and the cooler Indian subcontinent, which created anomalous
597 subsidence over the Indian region.

598 The reduction in the summer monsoon precipitation in the LGM simulation is
599 consistent with climate models and proxy records of monsoon precipitation (Liu et al.



2021; Jiang et al. 2015; Wang et al. 2023; Yan et al. 2016; Cao et al. 2019). The simulated northward shift of the ITCZ in our iCESM results, likely due to increased tropical North Pacific precipitation, conflicts with the southward shift simulated by several other models (Wang et al. 2023). This discrepancy points to uncertainties in climate simulations and suggests that more studies are required to assess the representation of tropical ocean-atmosphere interactions under the glacial climate conditions.

We also note that the low-level circulation responses in the LGM simulation (enhanced cyclonic barotropic shear with enhanced westerly anomalies over Southern India, and easterlies over the northern latitudes) is consistent with the climate model responses in future warming scenarios (Menon et al. 2013). Menon et al. (2013) find that under the RCP8.5 scenario, CMIP5 models project a weaker low level cyclonic monsoon circulation with enhanced westerly anomaly over northern India and easterly anomaly over the south, despite a simulated increase in the monsoon precipitation. Thus, our results are consistent with monsoon responses in future warming scenarios, such that in the colder LGM conditions, the monsoon precipitation is reduced due to thermodynamic response to cooling, while the dynamical response characterized by monsoon circulation indices in general is intensified.

A key contribution of this study is the novel application of water vapor source-tagging to the LGM climate simulation, which shows that the major water vapor sources for the Indian monsoon were unchanged between the pre-industrial and LGM climates. Our study finds that isotopic ratio of precipitation is enriched by ~1‰ over the ISM domain during the LGM, which is in agreement with Speleothem proxy records from Mawmluh (Dutt et al. 2015) and Bittoo caves (Kathayat et al. 2016) in North India. Our analysis confirms the amount effect (Dansgaard 1964) was not the primary driver for this enrichment, as we find no significant correlation between the changes in precipitation and $\delta^{18}\text{O}_{\text{precip}}$ from the PI to the LGM. Instead, our decomposition analysis using water vapor tagging finds that the simulated LGM enrichment is due to a reduced relative contribution from distant, isotopically depleted moisture sources and decreased rainout from Indian Ocean sources. The results are in agreement with studies by Tabor et al. (2018) and Hu et al. (2019) who



632 find the importance of different water vapor sources for the South Asian and East
633 Asian monsoon $\delta^{18}\text{O}_{\text{precip}}$ values. Hence, this study emphasizes that rather than
634 being a simple proxy for local rainfall, the $\delta^{18}\text{O}_{\text{precip}}$ values in the ISM region is a
635 complex signal integrating large-scale atmospheric dynamics and moisture sources.
636 Further, these findings pose questions for the interpretation of paleoclimate records
637 where $\delta^{18}\text{O}$ values of climate records are used as a direct proxy for local
638 precipitation intensity.

639 We note that our study has a few limitations. The version of the CESM model we
640 used has high climate sensitivity and overestimates the LGM global cooling (Zhu et
641 al. 2022), an issue attributed to its cloud parameterization. However, we suggest that
642 these biases do not affect our key results, as the model is able to both successfully
643 capture the present-day monsoon circulation, and isotopic distribution. The model is
644 also able to simulate the isotopic enrichment found in proxy records during the LGM.
645 Further, we use a single model, with prescribed SSTs and prescribed surface ocean
646 water isotope ratios because of the cost of computation when we utilize the water-
647 tagging capabilities of the model. Future work should employ fully coupled Earth
648 system models within a multi-model framework to investigate ocean-atmosphere-
649 isotope feedback and test the robustness of these results.

650 In conclusion, this study disentangles the drivers of Indian monsoon precipitation and
651 its isotopic signature during the LGM. The results highlight that the isotopic
652 composition of precipitation in the Indian monsoon region is a complex signal
653 integrating changes in circulation, changes in relative contribution of water vapor
654 sources, and upstream rainout processes. These findings underscore the importance
655 of considering moisture source and transport history when interpreting paleoclimate
656 isotope records from the Indian monsoon and other tropical monsoon regions.

657 **Code/Data availability**

658 The datasets used in the current study will be made available to the public.

659 **Author contributions**



660 TT: Conceptualization, Funding acquisition, Methodology, Investigation, Formal
 661 analysis, Visualization, Writing - Original Draft. GB: Methodology, Analysis, Writing -
 662 Review & Editing. JN: Methodology, Model software, Analysis, Writing - Review &
 663 Editing.

664 **Competing interests**

665 None of the authors has any competing interests.

666 **Acknowledgements**

667 TT is supported by the DST-INSPIRE Faculty Fellowship awarded by the
 668 Department of Science and Technology, India and Anusandhan National Research
 669 Foundation (ANRF) Early Career Research Grant. We acknowledge Jiang Zhu
 670 (NCAR) for providing the boundary conditions for the simulations, and we would like
 671 to thank Dr. André Paul for discussions during the initial stages of this research. We
 672 acknowledge the high-performance computing support from the Supercomputer
 673 Education and Research Centre (SERC), Indian Institute of Science, Bangalore. All
 674 the figures in the manuscript were created with NCL (NCAR Command Language
 675 Version 6.6.2, <http://www.ncl.ucar.edu/>).

676 **References:**

- 677 Adler, R. F., M. Sapiiano, G. J. Huffman, J. Wang, G. Gu, D. Bolvin, L. Chiu, et al.
 678 2018. "The Global Precipitation Climatology Project (GPCP) Monthly Analysis
 679 (New Version 2.3) and a Review of 2017 Global Precipitation." *Atmosphere* 9
 680 (4). <https://doi.org/10.3390/atmos9040138>.
 681 Annamalai, H., Jan Hafner, K. P. Sooraj, and P. Pillai. 2013. "Global Warming Shifts
 682 the Monsoon Circulation, Drying South Asia." *Journal of Climate* 26 (9): 2701–
 683 18.
 684 Azhar, Siti Syairah Atiqah, Sheeba Nettukandy Chenoli, Azizan Abu Samah, Seong-
 685 Joong Kim, and Nuncio Murukesh. 2023. "The Mechanism Linking the Variability
 686 of the Antarctic Sea Ice Extent in the Indian Ocean Sector to Indian Summer
 687 Monsoon Rainfall." *Climate Dynamics* 60 (9-10): 2665–85.
 688 Bartlein, P. J., S. P. Harrison, S. Brewer, S. Connor, B. A. S. Davis, K. Gajewski, J.



- 689 Guiot, et al. 2011. "Pollen-Based Continental Climate Reconstructions at 6 and
 690 21 Ka: A Global Synthesis." *Climate Dynamics* 37 (3-4): 775–802.
- 691 Bailey, Adriana, David Noone, Sylvia G. Dee, Jesse Nusbaumer, Jessica L. Conroy,
 692 Samantha Stevenson, and Alyssa Atwood. "Toward a process-oriented
 693 understanding of water in the climate system: recent insights from stable
 694 isotopes." *Environmental Research: Climate* (2024).
- 695 Boos, William R., and Kerry A. Emanuel. 2009. "Annual Intensification of the Somali
 696 Jet in a Quasi-equilibrium Framework: Observational Composites." *Quarterly
 697 Journal of the Royal Meteorological Society. Royal Meteorological Society
 698 (Great Britain)* 135 (639): 319–35.
- 699 Brady, E., S. Stevenson, D. Bailey, and Z. Liu. 2019. "The Connected Isotopic Water
 700 Cycle in the Community Earth System Model Version 1." *Journal of Advances*.
 701 <https://agupubs.onlinelibrary.wiley.com/doi/abs/10.1029/2019MS001663>.
- 702 Breitenbach, Sebastian F. M., Jess F. Adkins, Hanno Meyer, Norbert Marwan,
 703 Kanikicharla Krishna Kumar, and Gerald H. Haug. 2010. "Strong Influence of
 704 Water Vapor Source Dynamics on Stable Isotopes in Precipitation Observed in
 705 Southern Meghalaya, NE India." *Earth and Planetary Science Letters* 292 (1):
 706 212–20.
- 707 Broccoli, A. J., and S. Manabe. "The influence of continental ice, atmospheric CO₂,
 708 and land albedo on the climate of the last glacial maximum." *Climate dynamics*
 709 1, no. 2 (1987): 87–99.
- 710 Broccoli, A. J., and S. Manabe. 2008. "The effects of the Laurentide ice sheet on
 711 North American climate during the last glacial maximum." *Géographie physique
 712 et quaternaire* 41 (2): 291–99.
- 713 Brovkin, Victor, Edward Brook, John W. Williams, Sebastian Bathiany, Timothy M.
 714 Lenton, Michael Barton, Robert M. DeConto, et al. 2021. "Past Abrupt Changes,
 715 Tipping Points and Cascading Impacts in the Earth System." *Nature Geoscience*
 716 14 (8): 550–58.
- 717 Cao, Jian, Bin Wang, and Libin Ma. 2019. "Attribution of Global Monsoon Response
 718 to the Last Glacial Maximum Forcings." *Journal of Climate* 32 (19): 6589–6605.
- 719 Chakraborty, Supriyo, Aharna Sarkar, Amey Datye, V. Praveen, Pramit Kumar Deb
 720 Burman, Yashas Shivamurthy, Nibedita Samal et al. "Precipitation isotopes and
 721 monsoon dynamics in the core monsoon zone of India." *Scientific Reports* 15,
 722 no. 1 (2025): 6761.



- 723 Chen, Ziming, Tianjun Zhou, Lixia Zhang, Xiaolong Chen, Wenxia Zhang, and Jie
- 724 Jiang. 2020. "Global Land Monsoon Precipitation Changes in CMIP6
- 725 Projections." *Geophysical Research Letters* 47 (14).
- 726 <https://doi.org/10.1029/2019gl086902>.
- 727 Chou, Chia, and Chia-Wei Lan. 2012. "Changes in the Annual Range of Precipitation
- 728 under Global Warming." *Journal of Climate* 25 (1): 222–35.
- 729 Chou, Chia, J. David Neelin, Chao-An Chen, and Jien-Yi Tu. 2009. "Evaluating the
- 730 'rich-Get-Richer' Mechanism in Tropical Precipitation Change under Global
- 731 Warming." *Journal of Climate* 22 (8): 1982–2005.
- 732 Contreras-Rosales, L. A., and T. Jennerjahn. 2014. "Evolution of the Indian Summer
- 733 Monsoon and Terrestrial Vegetation in the Bengal Region during the Past 18
- 734 Ka." *Quaternary Science Reviews*.
- 735 https://www.sciencedirect.com/science/article/pii/S0277379114003242?casa_to
- 736 [ken=aiCf2W3kwWoAAAAA:RuWH7AnsDqErlfnmonRPsagJObV6-](https://www.sciencedirect.com/science/article/pii/S0277379114003242?casa_to)
- 737 [9b9whwrVSr6rj7yPvRiVPyzf-7c3hwkc1qzyjF1fdu52zu0](https://www.sciencedirect.com/science/article/pii/S0277379114003242?casa_to).
- 738 Dansgaard, W. 1964. "Stable Isotopes in Precipitation." *Tell'Us* 16 (4): 436–68.
- 739 Dee, Sylvia, Adriana Bailey, Jessica L. Conroy, Alyssa Atwood, Samantha
- 740 Stevenson, Jesse Nusbaumer, and David Noone. 2023. "Water Isotopes,
- 741 Climate Variability, and the Hydrological Cycle: Recent Advances and New
- 742 Frontiers." *Environmental Research: Climate* 2 (2): 022002.
- 743 Devaraju, N., Govindasamy Bala, and Angshuman Modak. 2015. "Effects of Large-
- 744 Scale Deforestation on Precipitation in the Monsoon Regions: Remote versus
- 745 Local Effects." *Proceedings of the National Academy of Sciences of the United*
- 746 *States of America* 112 (11): 3257–62.
- 747 Dey, Dipanjan, and Kristofer Döös. 2021. "Tracing the Origin of the South Asian
- 748 Summer Monsoon Precipitation and Its Variability Using a Novel Lagrangian
- 749 Framework." *Journal of Climate* 34 (21): 8655–68.
- 750 DiNezio, Pedro N., Jessica E. Tierney, Bette L. Otto-Bliesner, Axel Timmermann,
- 751 Tripti Bhattacharya, Nan Rosenbloom, and Esther Brady. 2018. "Glacial
- 752 Changes in Tropical Climate Amplified by the Indian Ocean." *Science Advances*
- 753 4 (12): eaat9658.
- 754 Duplessy, Jean-Claude, Laurent Labeyrie, and Claire Waelbroeck. 2002.
- 755 "Constraints on the Ocean Oxygen Isotopic Enrichment between the Last
- 756 Glacial Maximum and the Holocene: Paleoceanographic Implications."



- 757 *Quaternary Science Reviews* 21 (1-3): 315–30.
- 758 Dutt, Som, Anil K. Gupta, Steven C. Clemens, Hai Cheng, Raj K. Singh, Gayatri
 759 Kathayat, and R. Lawrence Edwards. 2015. “Abrupt Changes in Indian Summer
 760 Monsoon Strength during 33,800 to 5500 Years B.P.” *Geophysical Research*
 761 *Letters* 42 (13): 5526–32.
- 762 Fasullo, J., and P. J. Webster. 2003. “A Hydrological Definition of Indian Monsoon
 763 Onset and Withdrawal.” *Journal of Climate* 16 (19): 3200–3211.
- 764 Gadgil, Sulochana. 2003. “The Indian Monsoon and Its Variability.” *Annual Review of*
 765 *Earth and Planetary Sciences* 31 (1): 429–67.
- 766 Galewsky, Joseph, Hans Christian Steen-Larsen, Robert D. Field, John Worden,
 767 Camille Risi, and Matthias Schneider. 2016. “Stable Isotopes in Atmospheric
 768 Water Vapor and Applications to the Hydrologic Cycle.” *Reviews of Geophysics*
 769 54 (4): 809–65.
- 770 Geen, Ruth, Simona Bordoni, David S. Battisti, and Katrina Hui. 2020. “Monsoons,
 771 ITCZs, and the Concept of the Global Monsoon.” *Reviews of Geophysics* 58
 772 (4). <https://doi.org/10.1029/2020rg000700>.
- 773 Gimeno, Luis, Anita Drumond, Raquel Nieto, Ricardo M. Trigo, and Andreas Stohl.
 774 2010. “On the Origin of Continental Precipitation.” *Geophysical Research Letters*
 775 37 (13). <https://doi.org/10.1029/2010gl043712>.
- 776 Gimeno, Luis, Andreas Stohl, Ricardo M. Trigo, Francina Dominguez, Kei
 777 Yoshimura, Lisan Yu, Anita Drumond, Ana María Durán-Quesada, and Raquel
 778 Nieto. 2012. “Oceanic and Terrestrial Sources of Continental Precipitation.”
 779 *Reviews of Geophysics* 50 (4). <https://doi.org/10.1029/2012rg000389>.
- 780 Hanf, Franziska S., and H. Annamalai. 2020. “Systematic Errors in South Asian
 781 Monsoon Precipitation: Process-Based Diagnostics and Sensitivity to
 782 Entrainment in NCAR Models.” *Journal of Climate* 33 (7): 2817–40.
- 783 He, C., Z. Liu, B. L. Otto-Bliesner, E. C. Brady, C. Zhu, R. Tomas, P. U. Clark, et al.
 784 2021. “Hydroclimate Footprint of Pan-Asian Monsoon Water Isotope during the
 785 Last Deglaciation.” *Science Advances* 7 (4).
 786 <https://doi.org/10.1126/sciadv.abe2611>.
- 787 Hoffmann, G., and M. Heimann. 1997. “Water Isotope Modeling in the Asian
 788 Monsoon Region.” *Quaternary International* 37:115–28.
- 789 Hu, Jun, Julien Emile-Geay, Clay Tabor, Jesse Nusbaumer, and Judson Partin.
 790 2019. “Deciphering Oxygen Isotope Records from Chinese Speleothems with an



- 791 Isotope-enabled Climate Model." *Paleoceanography and Paleoclimatology* 34
- 792 (12): 2098–2112.
- 793 Jiang, Dabang, Zhiping Tian, Xianmei Lang, Masa Kageyama, and Gilles Ramstein.
- 794 2015. "The Concept of Global Monsoon Applied to the Last Glacial Maximum: A
- 795 Multi-Model Analysis." *Quaternary Science Reviews* 126 (October):126–39.
- 796 Kageyama, Masa, Pascale Braconnot, Cristiano M. Chiessi, Kira Rehfeld, Yassine
- 797 Ait Brahimi, Marina Dütsch, Benjamin Gwinneth, et al. 2024. "Lessons from
- 798 Paleoclimates for Recent and Future Climate Change: Opportunities and
- 799 Insights." *Frontiers in Climate* 6 (December).
- 800 <https://doi.org/10.3389/fclim.2024.1511997>.
- 801 Kageyama, Masa, and PMIP4 LGM group. 2020. "The PMIP4-CMIP6 Last Glacial
- 802 Maximum Experiments: Preliminary Results and Comparison with the PMIP3-
- 803 CMIP5 Simulations." <https://doi.org/10.5194/egusphere-egu2020-11153>.
- 804 Kathayat, Gayatri, Hai Cheng, Ashish Sinha, Christoph Spötl, R. Lawrence Edwards,
- 805 Haiwei Zhang, Xianglei Li, et al. 2016. "Indian Monsoon Variability on Millennial-
- 806 Orbital Timescales." *Scientific Reports* 6 (April):24374.
- 807 Kathayat, Gayatri, Ashish Sinha, Masahiro Tanoue, Kei Yoshimura, Hanying Li,
- 808 Haiwei Zhang, and Hai Cheng. 2021. "Interannual Oxygen Isotope Variability in
- 809 Indian Summer Monsoon Precipitation Reflects Changes in Moisture Sources."
- 810 *Communications Earth & Environment* 2 (1): 1–10.
- 811 Katzenberger, Anja, Jacob Schewe, Julia Pongratz, and Anders Levermann. 2021.
- 812 "Robust Increase of Indian Monsoon Rainfall and Its Variability under Future
- 813 Warming in CMIP6 Models." *Earth System Dynamics* 12 (2): 367–86.
- 814 Kaushal, N., S. Breitenbach, F. Lechleitner, A. Sinha, V. Tewari, S. M. Ahmad, M.
- 815 Berkelhammer, et al. 2018. "The Indian Summer Monsoon from a Speleothem
- 816 $\delta^{18}\text{O}$ perspective—A Review." *Quaternary*, September.
- 817 <https://doi.org/10.3390/QUAT1030029>.
- 818 K. Mukherjee, Sumit, Ayantika Dey Choudhury, and Raghavan Krishnan. 2024.
- 819 "Heavy-Precipitating Mid-Tropospheric Cyclonic Systems of the Indian Summer
- 820 Monsoon in a Warming Climate." <https://doi.org/10.5194/egusphere-egu24-268>.
- 821 Konecky, B. L., D. C. Noone, and K. M. Cobb. "The influence of competing
- 822 hydroclimate processes on stable isotope ratios in tropical rainfall." *Geophysical*
- 823 *Research Letters* 46, no. 3 (2019): 1622-1633.
- 824 Kong, Yunqi, Yuting Wu, Xiaoming Hu, Yana Li, and Song Yang. 2022. "Uncertainty



- 825 in Projections of the South Asian Summer Monsoon under Global Warming by
 826 CMIP6 Models: Role of Tropospheric Meridional Thermal Contrast.”
 827 *Atmospheric and Oceanic Science Letters* 15 (1): 100145.
- 828 Kripalani, R. H., J. H. Oh, A. Kulkarni, S. S. Sabade, and H. S. Chaudhari. 2007.
 829 “South Asian Summer Monsoon Precipitation Variability: Coupled Climate Model
 830 Simulations and Projections under IPCC AR4.” *Theoretical and Applied*
 831 *Climatology* 90 (3-4): 133–59.
- 832 Krishnan, R., T. P. Sabin, R. Vellore, M. Mujumdar, J. Sanjay, B. N. Goswami, F.
 833 Hourdin, J-L Dufresne, and P. Terray. 2016. “Deciphering the Desiccation Trend
 834 of the South Asian Monsoon Hydroclimate in a Warming World.” *Climate*
 835 *Dynamics* 47 (3-4): 1007–27.
- 836 Krishnan, R., J. Sanjay, Chellappan Gnanaseelan, Milind Mujumdar, Ashwini
 837 Kulkarni, and Supriyo Chakraborty. 2020. “Assessment of Climate Change over
 838 the Indian Region: A Report of the Ministry of Earth Sciences (MOES),
 839 Government of India,” 226.
- 840 Lambeck, K. 2000. “Global Ice Volumes at the Last Glacial Maximum and Early
 841 Lateglacial.” *Earth and Planetary Science Letters* 181 (4): 513–27.
- 842 Lambeck, Kurt, Hélène Rouby, Anthony Purcell, Yiyang Sun, and Malcolm
 843 Sambridge. 2014. “Sea Level and Global Ice Volumes from the Last Glacial
 844 Maximum to the Holocene.” *Proceedings of the National Academy of Sciences*
 845 *of the United States of America* 111 (43): 15296–303.
- 846 Lee, Jung-Eun, and Inez Fung. 2008. “‘Amount Effect’ of Water Isotopes and
 847 Quantitative Analysis of Post-Condensation Processes.” *Hydrological Processes*
 848 22 (1): 1–8.
- 849 LeGrande, A. N., and G. A. Schmidt. 2006. “Global Gridded Data Set of the Oxygen
 850 Isotopic Composition in Seawater.” *Geophysical Research Letters* 12 (33).
 851 <https://doi.org/10.1029/2006GL026011>.
- 852 Lewis, S. C., A. N. LeGrande, M. Kelley, and G. A. Schmidt. 2010. “Water Vapour
 853 Source Impacts on Oxygen Isotope Variability in Tropical Precipitation during
 854 Heinrich Events.” *Climate of the Past* 6 (3): 325–43.
- 855 Liu, Shengfa, Wenxing Ye, Min-Te Chen, Hui-Juan Pan, Peng Cao, Hui Zhang,
 856 Somkiat Khokiattiwong, Narumol Kornkanitnan, and Xuefa Shi. 2021.
 857 “Millennial-Scale Variability of Indian Summer Monsoon during the Last 42 Kyr:
 858 Evidence Based on Foraminiferal Mg/Ca and Oxygen Isotope Records from the



- 859 Central Bay of Bengal." *Palaeogeography, Palaeoclimatology, Palaeoecology*
 860 562 (January):110112.
- 861 Liu, Z., X. Wen, E. C. Brady, B. Otto-Bliesner, and G. Yu. 2014. "Chinese Cave
 862 Records and the East Asia Summer Monsoon." *Quaternary Science Reviews*.
 863 https://www.sciencedirect.com/science/article/pii/S0277379113004150?casa_to
 864 [ken=8RYar31ITq8AAAAA:vX8ZUyWAR_oJN_4Qie3b5WlxdKkgm1q_SpDVIUS-](https://www.sciencedirect.com/science/article/pii/S0277379113004150?casa_to)
 865 [cXBN0-6aFKZRgflTYitdt9ljs5naycMenuqt.](https://www.sciencedirect.com/science/article/pii/S0277379113004150?casa_to)
- 866 Li, Xiuping, Lei Wang, Shiyuan Zhong, and Liu Liu. 2024. "Comparative Analysis of
 867 Indices in Capturing the Onset and Withdrawal of the South Asian Summer
 868 Monsoon." *Environmental Research Communications* 6 (3): 031007.
- 869 Lohmann, Gerrit, Martin Butzin, Nina Eissner, Xiaoxu Shi, and Christian Stepanek.
 870 "Abrupt climate and weather changes across time scales." *Paleoceanography*
 871 *and Paleoclimatology* 35, no. 9 (2020): e2019PA003782.
- 872 Lofverstrom, Marcus, and Jiang Zhu. 2023. "Tropical Precipitation Woes in the
 873 Community Earth System Model Version 2." *Geophysical Research Letters* 50
 874 (21). <https://doi.org/10.1029/2023gl104416>.
- 875 Maher, B. A. 2008. "Holocene Variability of the East Asian Summer Monsoon from
 876 Chinese Cave Records: A Re-Assessment." *Holocene* 18 (6): 861–66.
- 877 MARGO Project Members. 2009. "Constraints on the Magnitude and Patterns of
 878 Ocean Cooling at the Last Glacial Maximum." *Nature Geoscience* 2 (2): 127–32.
- 879 McGee, David. "Glacial–interglacial precipitation changes." *Annual Review of Marine*
 880 *Science* 12, no. 1 (2020): 525–557.
- 881 McGee, David, Aaron Donohoe, John Marshall, and David Ferreira. 2014. "Changes
 882 in ITCZ Location and Cross-Equatorial Heat Transport at the Last Glacial
 883 Maximum, Heinrich Stadial 1, and the Mid-Holocene." *Earth and Planetary*
 884 *Science Letters* 390 (March):69–79.
- 885 Nusbaumer, J., T. E. Wong, and C. Bardeen. 2017. "Evaluating Hydrological
 886 Processes in the Community Atmosphere Model Version 5 (CAM5) Using
 887 Stable Isotope Ratios of Water." *Journal of Advances in*.
 888 <https://agupubs.onlinelibrary.wiley.com/doi/abs/10.1002/2016MS000839>.
- 889 Ordóñez, Paulina, Pedro Ribera, David Gallego, and Cristina Peña-Ortiz. 2012.
 890 "Major Moisture Sources for Western and Southern India and Their Role on
 891 Synoptic-Scale Rainfall Events." *Hydrological Processes* 26 (25): 3886–95.
- 892 Pathak, Amey, Subimal Ghosh, and Praveen Kumar. 2014. "Precipitation Recycling



- 893 in the Indian Subcontinent during Summer Monsoon.” *Journal of*
 894 *Hydrometeorology* 15 (5): 2050–66.
- 895 Pathak, Raju, Sandeep Sahany, Saroj Kanta Mishra, and S. K. Dash. 2019.
 896 “Precipitation Biases in CMIP5 Models over the South Asian Region.” *Scientific*
 897 *Reports* 9 (1): 9589.
- 898 Pausata, Francesco S. R., David S. Battisti, Kerim H. Nisancioglu, and Cecilia M.
 899 Bitz. 2011. “Chinese Stalagmite $\delta^{18}\text{O}$ Controlled by Changes in the Indian
 900 Monsoon during a Simulated Heinrich Event.” *Nature Geoscience* 4 (7): 474–80.
- 901 Peltier, W. R., D. F. Argus, and R. Drummond. 2015. “Space Geodesy Constrains
 902 Ice Age Terminal Deglaciation: The Global ICE-6G_C (VM5a) Model.” *Journal of*
 903 *Geophysical Research. Solid Earth* 120 (1): 450–87.
- 904 P J, Vidya, M. Ravichandran, M. P. Subeesh, Sourav Chatterjee, and Nuncio M.
 905 2020. “Global Warming Hiatus Contributed Weakening of the Mascarene High in
 906 the Southern Indian Ocean.” *Scientific Reports* 10 (1): 3255.
- 907 Rehfeld, Kira, Raphaël Hébert, Juan M. Lora, Marcus Lofverstrom, and Chris M.
 908 Brierley. “Variability of surface climate in simulations of past and future.” *Earth*
 909 *System Dynamics* 11, no. 2 (2020): 447-468.
- 910 Risi, Camille, Sandrine Bony, and Françoise Vimeux. 2008. “Influence of Convective
 911 Processes on the Isotopic Composition ($\delta^{18}\text{O}$ and δD) of Precipitation and Water
 912 Vapor in the Tropics: 2. Physical Interpretation of the Amount Effect.” *Journal of*
 913 *Geophysical Research*. <https://doi.org/10.1029/2008jd009943>.
- 914 Roxy, Mathew Koll, Kapoor Ritika, Pascal Terray, Raghu Murtugudde, Karumuri
 915 Ashok, and B. N. Goswami. 2015. “Drying of Indian Subcontinent by Rapid
 916 Indian Ocean Warming and a Weakening Land-Sea Thermal Gradient.” *Nature*
 917 *Communications* 6 (1): 1–10.
- 918 Seltzer, A. M., P. W. Davidson, S. A. Shackleton, D. P. Nicholson, and S. Khatiwala.
 919 2024. “Global Ocean Cooling of 2.3°C during the Last Glacial Maximum.”
 920 *Geophysical Research Letters* 51 (9). <https://doi.org/10.1029/2024gl108866>.
- 921 Shewale, M. P., and Shravan Kumar. 2005. “CLIMATOLOGICAL FEATURES OF
 922 DROUGHT INCIDENCES IN INDIA.”
 923 <https://imd pune.gov.in/Reports/drought.pdf>.
- 924 Sima, Adriana, André Paul, Michael Schulz, and Johannes Oerlemans. 2006.
 925 “Modeling the Oxygen-Isotopic Composition of the North American Ice Sheet
 926 and Its Effect on the Isotopic Composition of the Ocean during the Last Glacial



- 927 Cycle." *Geophysical Research Letters* 33 (15).
 928 <https://doi.org/10.1029/2006gl026923>.
 929 Sinha, Ashish, Gayatri Kathayat, Hai Cheng, Sebastian F. M. Breitenbach, Max
 930 Berkelhammer, Manfred Mudelsee, Jayant Biswas, and R. L. Edwards. 2015.
 931 "Trends and Oscillations in the Indian Summer Monsoon Rainfall over the Last
 932 Two Millennia." *Nature Communications* 6 (February):6309.
 933 Sjolte, Jesper, and Georg Hoffmann. 2014. "Modelling Stable Water Isotopes in
 934 Monsoon Precipitation during the Previous Interglacial." *Quaternary Science*
 935 *Reviews* 85 (February):119–35.
 936 Tabor, Clay R., Bette L. Otto-Bliesner, Esther C. Brady, Jesse Nusbaumer, Jiang
 937 Zhu, Michael P. Erb, Tony E. Wong, Zhengyu Liu, and David Noone. 2018.
 938 "Interpreting Precession-driven $\delta^{18}\text{O}$ Variability in the South Asian Monsoon
 939 Region." *Journal of Geophysical Research Atmospheres* 123 (11): 5927–46.
 940 Tharammal, Thejna, Govindasamy Bala, and David Noone. 2017. "Impact of Deep
 941 Convection on the Isotopic Amount Effect in Tropical Precipitation." *Journal of*
 942 *Geophysical Research Atmospheres* 122 (3): 1505–23.
 943 Tharammal, Thejna, Govindasamy Bala, and Jesse M. Nusbaumer. 2023. "Sources
 944 of Water Vapor and Their Effects on Water Isotopes in Precipitation in the Indian
 945 Monsoon Region: A Model-Based Assessment." *Scientific Reports* 13 (1): 708.
 946 Tharammal, Thejna, André Paul, Ute Merkel, and D. Noone. "Influence of Last
 947 Glacial Maximum boundary conditions on the global water isotope distribution in
 948 an atmospheric general circulation model." *Climate of the Past* 9, no. 2 (2013):
 949 789-809.
 950 Tierney, Jessica E., Christopher J. Poulsen, Isabel P. Montañez, Tripti Bhattacharya,
 951 Ran Feng, Heather L. Ford, Bärbel Hönlisch, et al. 2020. "Past Climates Inform
 952 Our Future." *Science* 370 (6517). <https://doi.org/10.1126/science.aay3701>.
 953 Tierney, Jessica E., Jiang Zhu, Jonathan King, Steven B. Malevich, Gregory J.
 954 Hakim, and Christopher J. Poulsen. 2020. "Glacial Cooling and Climate
 955 Sensitivity Revisited." *Nature* 584 (7822): 569–73.
 956 Tiwari, Manish, Ashutosh K. Singh, and Rengaswamy Ramesh. 2011. "High-
 957 Resolution Monsoon Records since Last Glacial Maximum: A Comparison of
 958 Marine and Terrestrial Paleoarchives from South Asia." *Journal of Geological*
 959 *Research* 2011 (August):1–12.
 960 Trenberth, K. E. 2011. "Changes in Precipitation with Climate Change." *Climate*



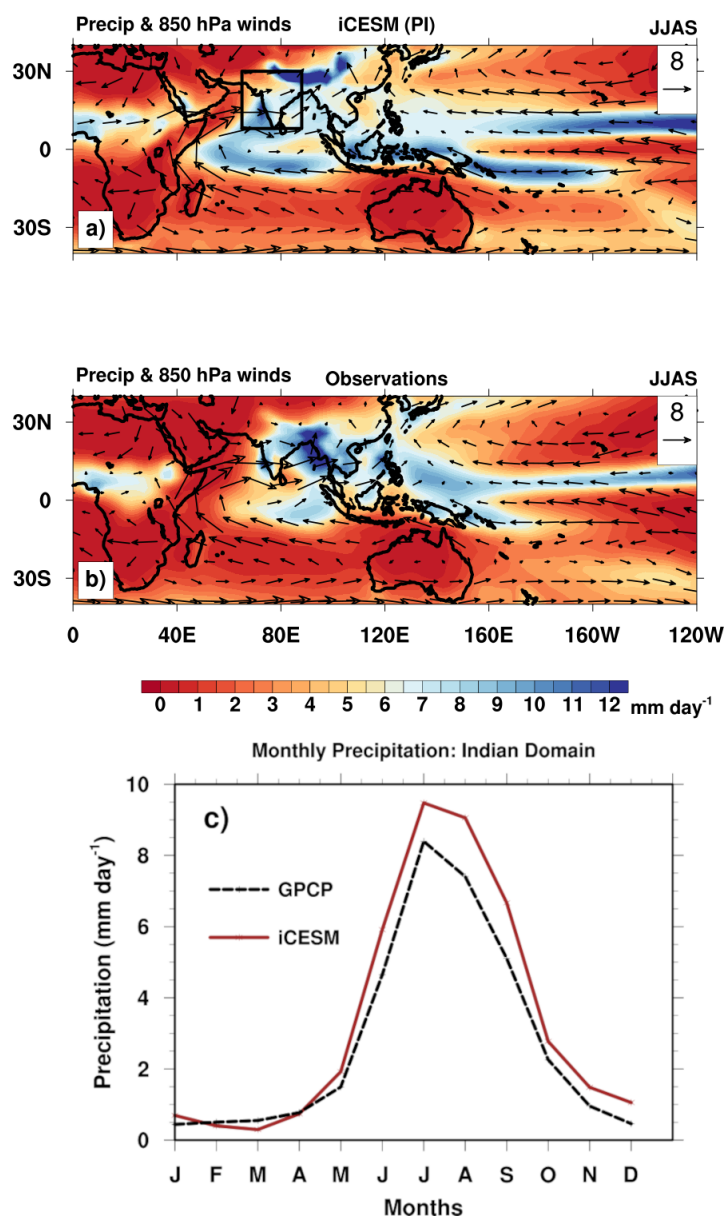
- 961 *Research* 47 (1): 123–38.
- 962 Wang, Bin, M. Biasutti, M. Byrne, C. Castro, Chih-Pei Chang, K. Cook, R. Fu, et al.
- 963 2020. “Monsoons Climate Change Assessment.” *Bulletin of the American*
- 964 *Meteorological Society* 102 (1): E1–19.
- 965 Wang, Ting, Na Wang, and Dabang Jiang. 2023. “Last Glacial Maximum ITCZ
- 966 Changes from PMIP3/4 Simulations.” *Journal of Geophysical Research*
- 967 *Atmospheres* 128 (10). <https://doi.org/10.1029/2022jd038103>.
- 968 Webster, Peter J., and Song Yang. 1992. “Monsoon and ENSO: Selectively
- 969 Interactive Systems.” *Quarterly Journal of the Royal Meteorological Society.*
- 970 *Royal Meteorological Society (Great Britain)* 118 (507): 877–926.
- 971 Weldeab, Syee, Carsten Rühlemann, Qinghua Ding, Vyacheslav Khon, Birgit
- 972 Schneider, and William R. Gray. 2022. “Impact of Indian Ocean Surface
- 973 Temperature Gradient Reversals on the Indian Summer Monsoon.” *Earth and*
- 974 *Planetary Science Letters* 578 (117327): 117327.
- 975 Windler, Grace, Jessica E. Tierney, Jiang Zhu, and Christopher J. Poulsen. 2020.
- 976 “Unraveling Glacial Hydroclimate in the Indo-pacific Warm Pool: Perspectives
- 977 from Water Isotopes.” *Paleoceanography and Paleoclimatology* 35 (12).
- 978 <https://doi.org/10.1029/2020pa003985>.
- 979 Xavier, Prince K., Charline Marzin, and B. N. Goswami. 2007. “An Objective
- 980 Definition of the Indian Summer Monsoon Season and a New Perspective on
- 981 the ENSO–monsoon Relationship.” *Quarterly Journal of the Royal*
- 982 *Meteorological Society. Royal Meteorological Society (Great Britain)* 133 (624):
- 983 749–64.
- 984 Xue, Feng, Huijun Wang, and Jinhai He. 2003. “Interannual Variability of Mascarene
- 985 High and Australian High and Their Influences on Summer Rainfall over East
- 986 Asia.” *Kexue Tongbao [Chinese Science Bulletin]* 48 (5): 492–97.
- 987 Yadava, M. G., R. Ramesh, and G. B. Pant. 2004. “Past Monsoon Rainfall Variations
- 988 in Peninsular India Recorded in a 331-Year-Old Speleothem.” *Holocene.*
- 989 <https://journals.sagepub.com/doi/pdf/10.1191/0959683604hl728rp>.
- 990 Yanase, W., and A. Abe-Ouchi. 2007. “The LGM Surface Climate and Atmospheric
- 991 Circulation over East Asia and the North Pacific in the PMIP2 Coupled Model
- 992 Simulations.” *Climate of the Past* 3 (3): 439–51.
- 993 Yan, Mi, Bin Wang, and Jian Liu. 2016. “Global Monsoon Change during the Last
- 994 Glacial Maximum: A Multi-Model Study.” *Climate Dynamics* 47 (1-2): 359–74.



- 995 Zhu, Jiang, Zhengyu Liu, Esther Brady, Bette Otto-Bliesner, Jiaxu Zhang, David
 996 Noone, Robert Tomas, et al. 2017. “Reduced ENSO Variability at the LGM
 997 Revealed by an Isotope-enabled Earth System Model.” *Geophysical Research*
 998 *Letters* 44 (13): 6984–92.
 999 Zhu, Jiang, Bette L. Otto-Bliesner, Esther C. Brady, Andrew Gettelman, Julio T.
 1000 Bacmeister, Richard B. Neale, Christopher J. Poulsen, Jonah K. Shaw, Zachary
 1001 S. McGraw, and Jennifer E. Kay. 2022. “LGM Paleoclimate Constraints Inform
 1002 Cloud Parameterizations and Equilibrium Climate Sensitivity in CESM2.” *Journal*
 1003 *of Advances in Modeling Earth Systems* 14 (4).
 1004 <https://doi.org/10.1029/2021ms002776>.
 1005 Zhu, Jiang, and Christopher J. Poulsen. 2021. “Last Glacial Maximum (LGM) Climate
 1006 Forcing and Ocean Dynamical Feedback and Their Implications for Estimating
 1007 Climate Sensitivity.” *Climate of the Past* 17 (1): 253–67.

1008
 1009
 1010
 1011
 1012
 1013
 1014
 1015
 1016
 1017
 1018
 1019

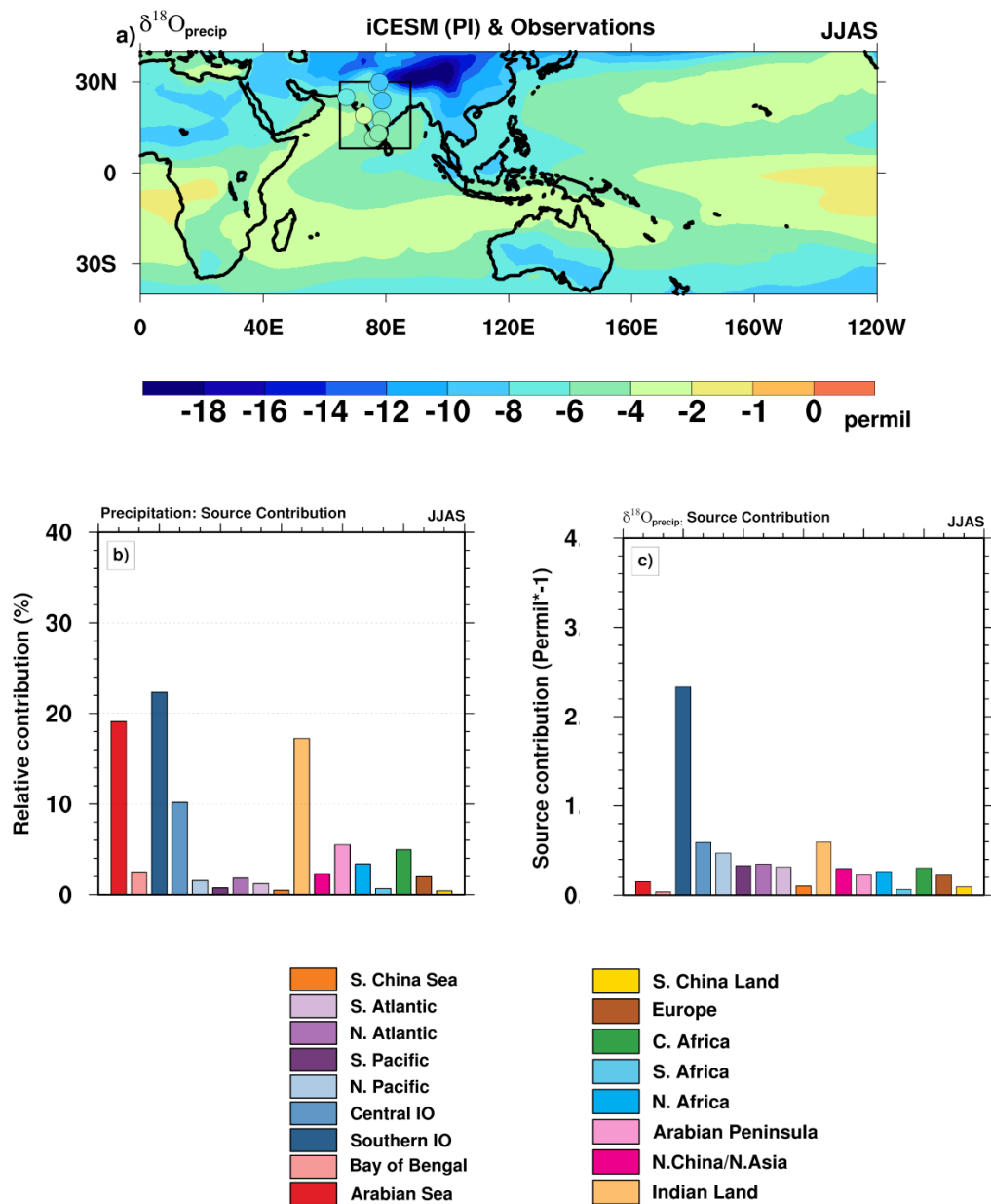
1020 **Main Figures**



1021
 1022 Figure 1: Model-simulated and observed precipitation (shaded, mm day⁻¹) and 850
 1023 hPa winds (vectors in m s⁻¹, reference vectors are shown in the panels) for the
 1024 summer monsoon season (mean of June-July-August-September-JJAS). Panel (a)
 1025 shows the simulated JJAS mean precipitation and 850 hPa winds from the iCESM
 1026 Pre-Industrial (PI) simulation. Panel (b) shows the corresponding JJAS long-term
 1027 mean precipitation from GPCP (Adler et al., 2018) and 850 hPa winds from ERA5
 1028 reanalysis (1980-2000; Hersbach et al., 2020). Panel (c) shows the monthly mean



1029 precipitation averaged over the land grid cells in the Indian domain (8°N-30°N, 65°E-
1030 88°E; black box in panel a, comparing the iCESM simulation with GPCP
1031 observations.
1032
1033
1034
1035
1036
1037



1038
1039 Figure 2: Isotopic composition of precipitation ($\delta^{18}\text{O}_{\text{precip}}$) for the Indian summer
1040 monsoon season in the pre-industrial (PI) simulation, shown along with relative
1041 contribution of precipitation from the tagged sources, and their $\delta^{18}\text{O}$ values in
1042 precipitation (weighted by relative contribution of precipitation).
1043 Panel (a) shows the mean JJAS $\delta^{18}\text{O}_{\text{precip}}$ (shading, in permil [‰]). The filled circles
1044 in the Indian domain (8°N-30°N, 65°E-88°E; shown in black box in panel a) represent



1045 long-term JJAS mean observational data from Global Network of Isotopes in
1046 Precipitation (GNIP) stations. Panel (b) shows the relative contribution ($P_{\text{tag}}/P_{\text{total}}$, in
1047 %) of precipitation to the Indian summer monsoon domain from 17 tagged water
1048 vapor source regions. Panel (c) shows the $\delta^{18}\text{O}_{\text{precip}}$ of tagged precipitation from the
1049 17 different source regions that contribute to the Indian monsoon precipitation. The
1050 y-axis values in panel (c) are multiplied by -1 for visualization purposes (units of ‰).

1051

1052

1053

1054

1055

1056

1057

1058

1059

1060

1061

1062

1063

1064

1065

1066

1067

1068

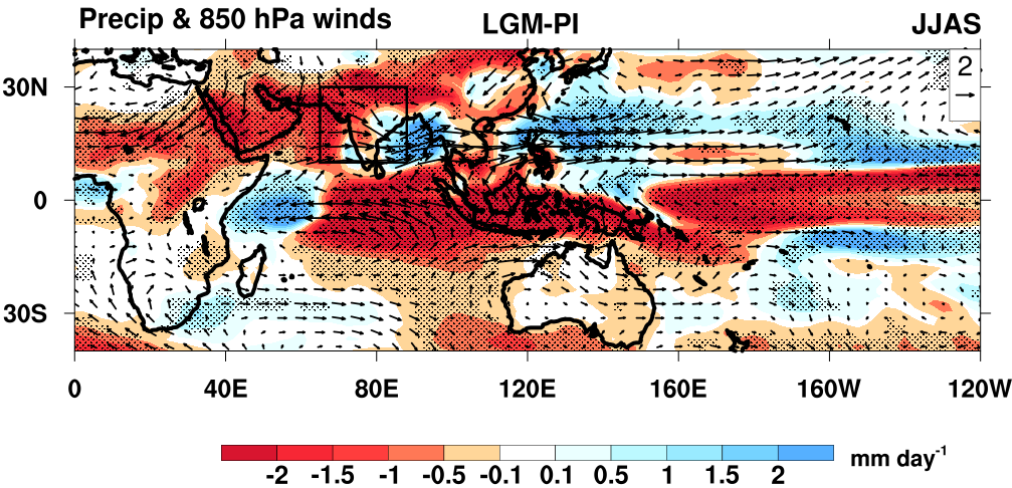
1069

1070

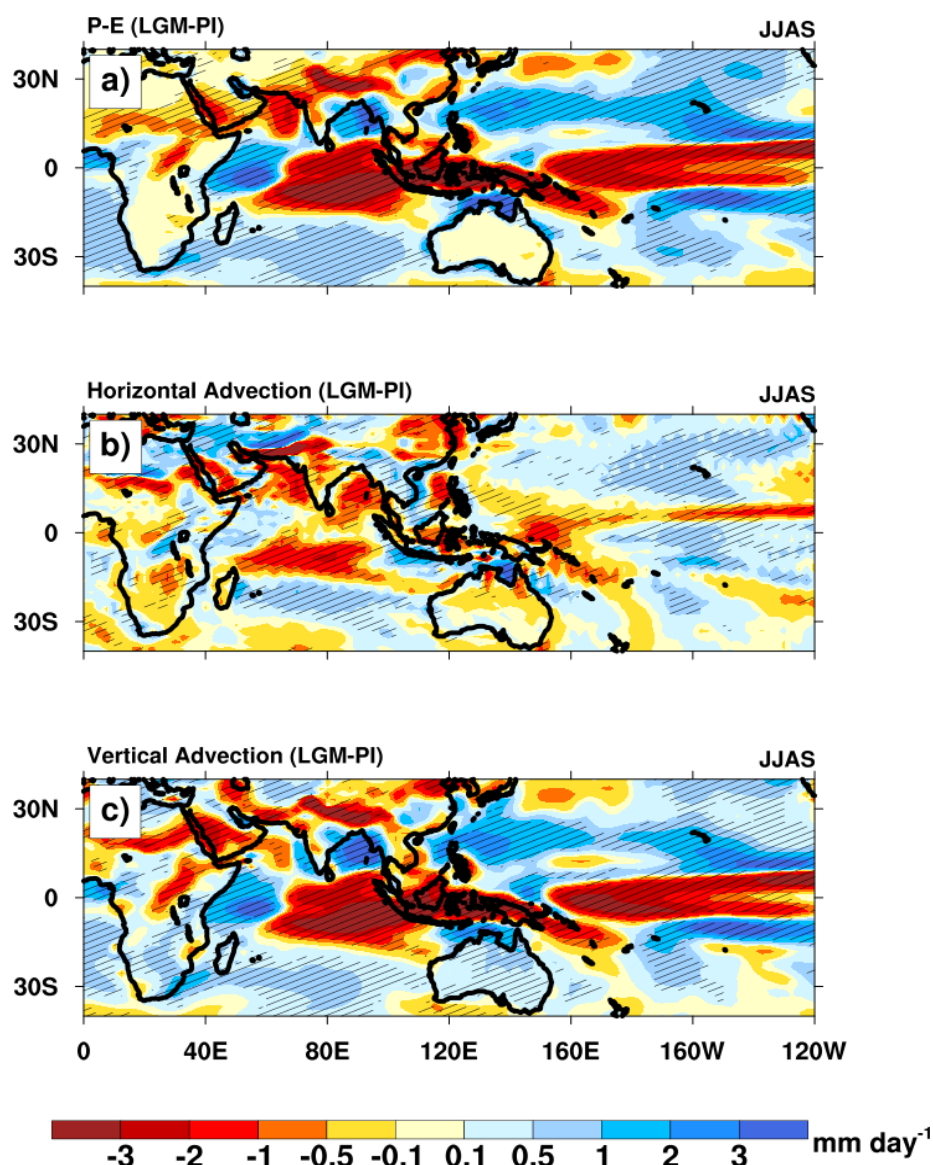
1071

1072

1073



1074
1075
1076 Figure 3: The simulated differences in JJAS mean precipitation (shaded, in mm
1077 day⁻¹) and low-level winds (850 hPa, vectors shown in m s⁻¹) between the pre-
1078 industrial and the Last Glacial Maximum (LGM) simulations, shown as LGM-PI.
1079 Regions where the anomalies are statistically significant at the 95% confidence level
1080 are stippled. Significance level is estimated using a Student's t test from a sample of
1081 20 annual means from the control and LGM simulations.
1082
1083
1084
1085
1086
1087



1088
 1089

1090 Figure 4: Changes in the JJAS mean atmospheric moisture budget between the
 1091 LGM and the PI simulations, shown as LGM-PI. The panels show the components of
 1092 the vertically integrated moisture budget anomaly: Panel a) shows anomalies in
 1093 precipitation minus evaporation (P-E). Panel b) shows anomaly in horizontal water
 1094 vapor advection ($-\langle \mathbf{v} \cdot \nabla q \rangle$). Panel c) shows anomaly in vertical water vapor
 1095 advection ($-\langle \omega \partial q / \partial p \rangle$). V is the horizontal wind, q specific humidity, p atmospheric
 1096 pressure, and ω pressure velocity. All panels have the units of mm day^{-1} . The



1097 hatching shows regions where the anomalies are statistically significant at the 95%
1098 confidence level. Significance level is estimated using a Student's t test from a
1099 sample of 20 annual means from the control and LGM simulations.

1100

1101

1102

1103

1104

1105

1106

1107

1108

1109

1110

1111

1112

1113

1114

1115

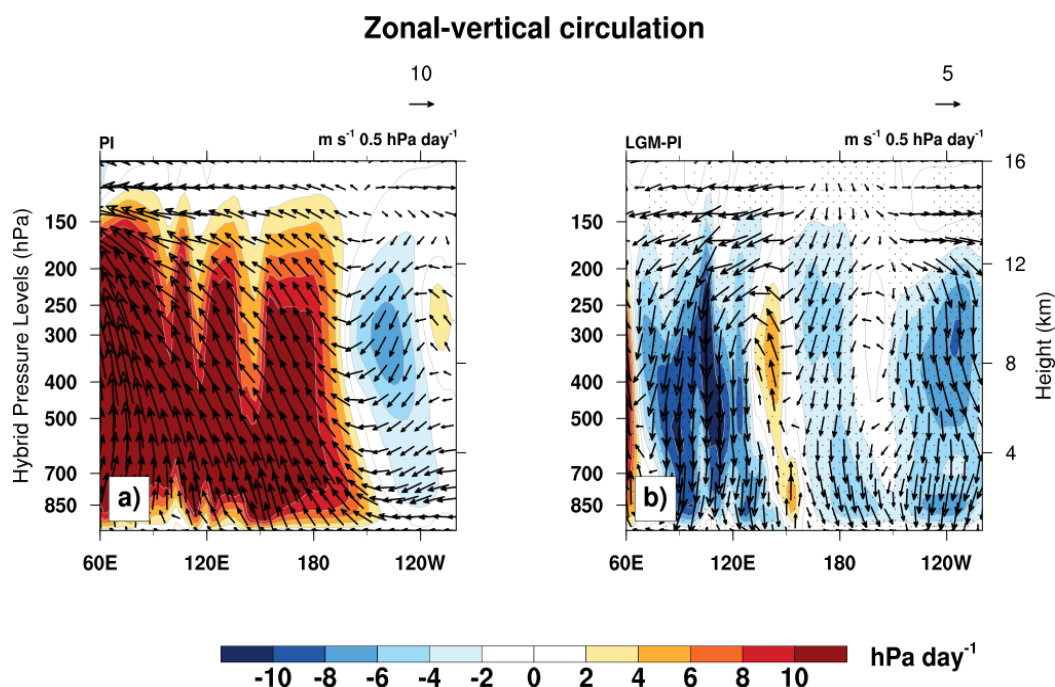
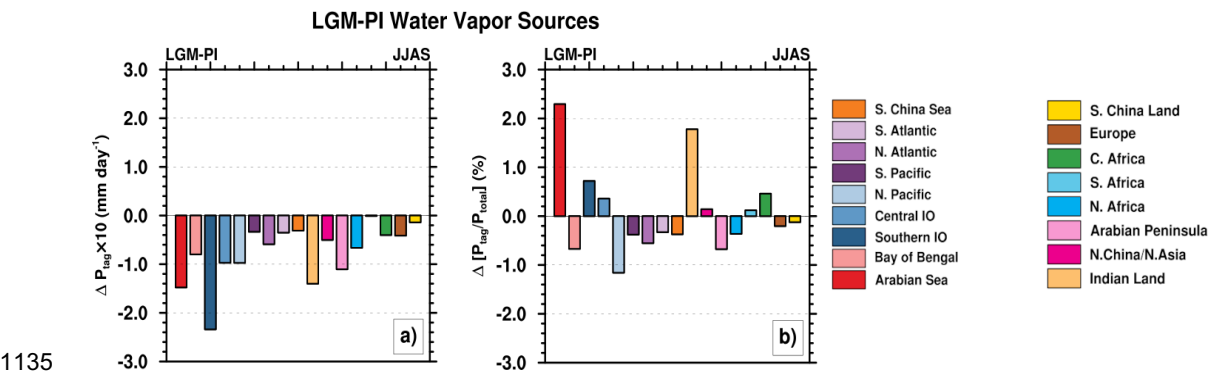


Figure 5: The tropical zonal circulation during the JJAS season, averaged between 10°S and 10°N. Panel a) shows the circulation in the PI control simulation, and the right panel b) shows the anomalies between the LGM and PI simulations (as LGM-PI). In both panels, shading represents the vertical pressure velocity ($-\omega$), where blue shading indicates downward motion and red shading indicates upward motion. The vectors show the zonal-vertical circulation, composed of zonal wind (u , in m s^{-1}) and vertical pressure velocity ($-\omega$), with the ω scaled by 0.5 hPa day^{-1} for visualization. The reference vectors are shown in the top right of the panels. The stippling in panel b) shows regions where the anomalies are statistically significant at the 95% confidence level. Significance level is estimated using a Student's t test from a sample of 20 annual means from the control and LGM simulations.



1132
1133
1134



1135

1136 Figure 6: Changes in the precipitation contribution from 17 tagged moisture source
1137 regions to the Indian monsoon domain's JJAS mean precipitation between the LGM
1138 and the PI simulations. The source regions corresponding to each bar are identified
1139 in the legend. Panel (a) shows the absolute difference in precipitation contribution
1140 from each source region (ΔP_{tag}). The values are shown in mm day^{-1} and have been
1141 scaled up by a factor of 10 for visualization. Panel (b) shows the difference in the
1142 relative contribution of each source to the total precipitation at the Indian monsoon
1143 domain ($\Delta [P_{\text{tag}}/P_{\text{total}}]$), shown as a percentage (%).

1144

1145

1146

1147

1148

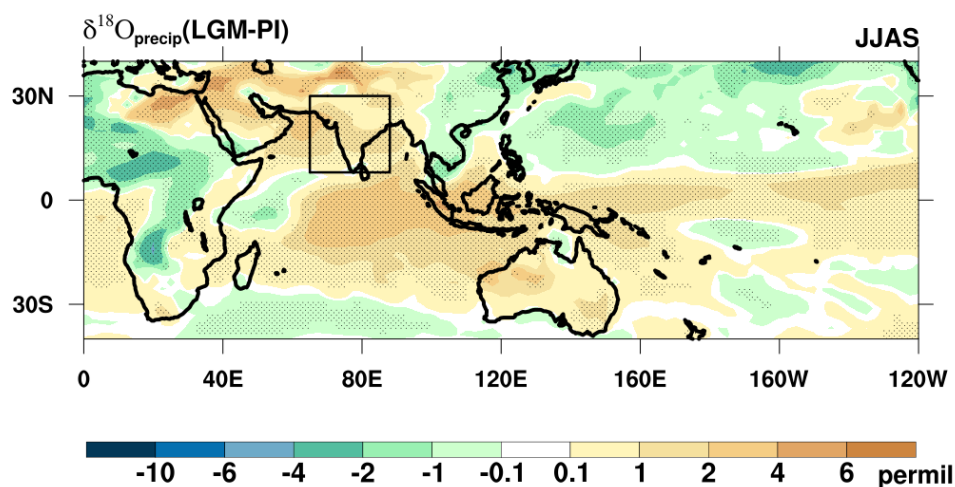
1149

1150

1151



1152



1153

1154 Figure 7: The anomalies of JJAS mean precipitation weighted $\delta^{18}\text{O}_{\text{precip}}$ in permil
 1155 between the LGM and PI simulations as LGM-PI. The Indian monsoon domain is
 1156 shown in a black box in the plot. Regions where the anomalies are statistically
 1157 significant at the 95% confidence level are stippled. Significance level is estimated
 1158 using a Student's t test from a sample of 20 annual means from the PI control and
 1159 LGM simulations.

1160

1161

1162

1163

1164

1165

1166

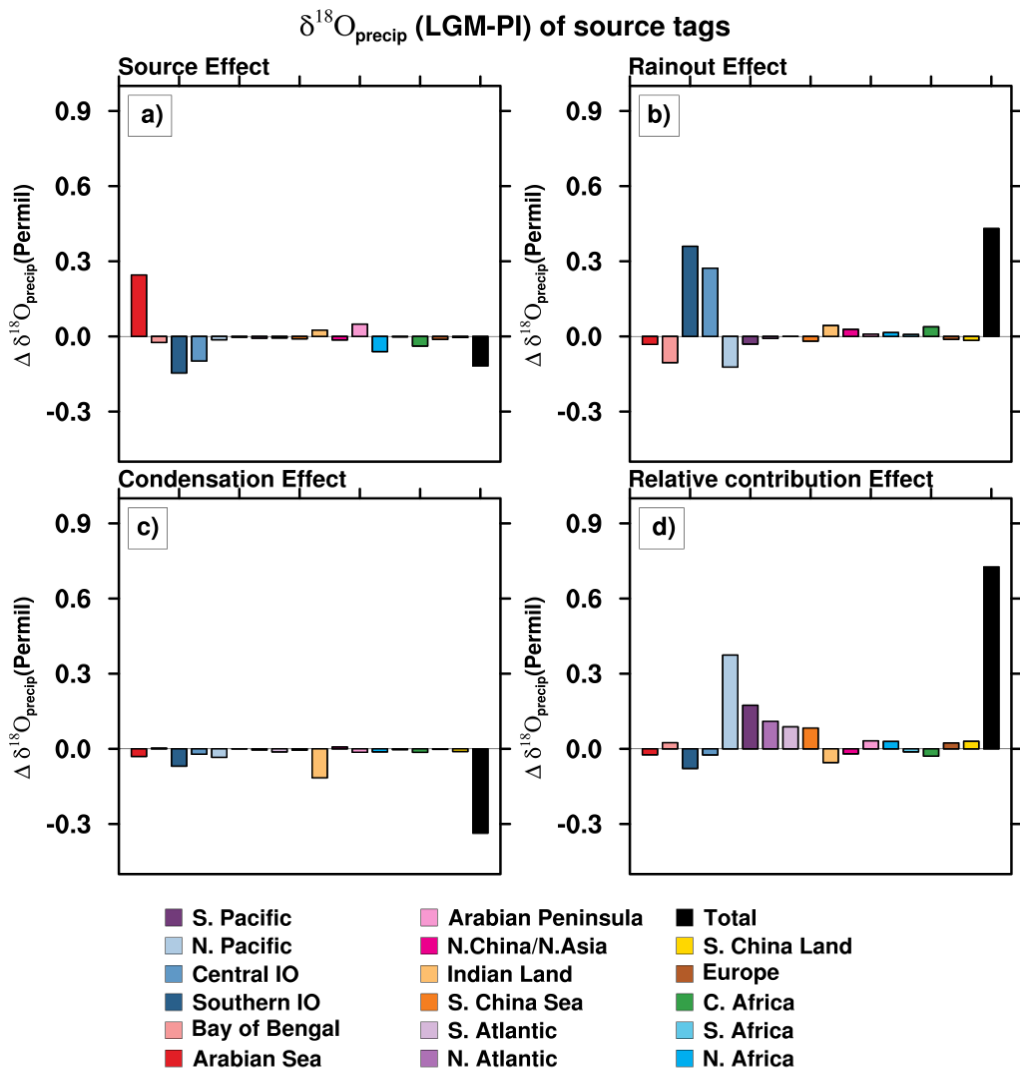
1167

1168



1169

1170



1171

1172 Figure 8: Decomposition of the change in JJAS mean precipitation $\delta^{18}\text{O}$ ($\Delta\delta^{18}\text{O}_{\text{precip}}$)
1173 for the Indian monsoon domain between the LGM and PI simulations. All values are
1174 in permil (‰). The $\Delta\delta^{18}\text{O}_{\text{precip}}$ is divided into contributions from 17 tagged moisture
1175 source regions, shown in the legend. The decomposition separates the total anomaly
1176 into four primary physical processes for each tag. Panel a) shows the Source Effect:
1177 Changes in the $\delta^{18}\text{O}$ of water vapor at its evaporative source. Panel b) shows the



1178 Rainout Effect: Changes in isotopic composition due to rainout during atmospheric
1179 transport from the source region to the ISM domain. Panel c) shows the
1180 Condensation Effect: Changes in the isotopic fractionation during the conversion of
1181 water vapor to precipitation over the monsoon region. Panel d) shows the
1182 Precipitation Relative Contribution Effect: Changes in $\delta^{18}\text{O}_{\text{precip}}$ for each tag resulting
1183 from shifts in the relative contribution of precipitation from different source regions.

1184

1185

1186

1187

1188